CrystEngComm

ROYAL SOCIETY OF CHEMISTRY

PAPER

View Article Online
View Journal

Cite this: DOI: 10.1039/d6ce00140h

Electron diffraction and crystal engineering of Pigment Red 5, $C_{30}H_{31}ClN_4O_7S$

Sylvia Reibeling, [a] Tatiana E. Gorelik, *[bc] Eiken Haussühl, [d] Nick Liebisch[a] and Martin U. Piepenbring †*[a]

Pigment Red 5 (P.R.5) is an industrial organic hydrazone pigment with non-optimal application properties. In its application media – paints and printing inks – the pigment is not dissolved, but finely dispersed; hence, the crystal structure is maintained and has a strong effect on the properties. Hitherto, the crystal structure of P.R.5 has not been known, because the pronounced insolubility in water and in common organic solvents hampers the growth of single crystals for X-ray analysis. Since structure determination from powder data failed as well, the structure was determined by 3-dimensional electron diffraction (3D-ED). P.R.5 crystallises in the triclinic space group $P\bar{1}$ (Z = 2), with layers of largely planar molecules. The structure was later confirmed by single-crystal X-ray analysis of a tiny crystal. The structure contains a void of about 36 Å^3 between the molecules—a feature unprecedented in any known commercial organic pigment, as such voids deteriorate the packing efficiency, the lattice energy, and the application properties. To address these drawbacks, crystal engineering strategies were applied. First, lattice-energy minimisations guided the selection of potential derivatives and solid solutions. Several promising solid solutions were then synthesised and analysed by X-ray powder diffraction and single crystal analysis, and, indeed, according to the lattice-energy minimisations, the void could be filled.

Received 13th February 2026,
Accepted 16th April 2026

DOI: 10.1039/d6ce00140h

rsc.li/crystengcomm

1. Introduction

Pigment Red 5 (P.R.5, $C_{30}H_{31}ClN_4O_7S$) is an industrial organic hydrazone pigment (see Scheme 1). P.R.5 offers a bluish-red shade, and is mainly used for the colouration of paints and printing inks, especially offset inks, packaging gravure inks and flexo inks.[1] It is also used for spin dyeing of fibres and for latex dipping.[2] Furthermore, P.R.5 is found in cosmetics such as lipstick and eye shadow. For cosmetics, an especially pure pigment grade is produced, and the corresponding batches are carefully tested according to all regulatory restrictions.[3]

Commercially, P.R.5 is available in different grades for the individual applications. For example, the company Sudarshan offers grades for paints and inks, an aqueous pigment preparation for water-based decorative paints, a pigment dispersion with propylene glycol used for the spin dyeing and latex dip, an aqueous pigment preparation for soap bars and cosmetics, a pigment dispersion with glycerine, used for products bearing eco-labels, and a microbiologically pure grade for chalks and finger paints, as well as personal care products, cosmetics, detergents and cleaners.[2]

P.R.5 exhibits a useful, clear carmine-red shade. However, the other application properties are not optimal: the light fastness (photostability) is only mediocre, which hampers its use in automotive finishes. The solvent

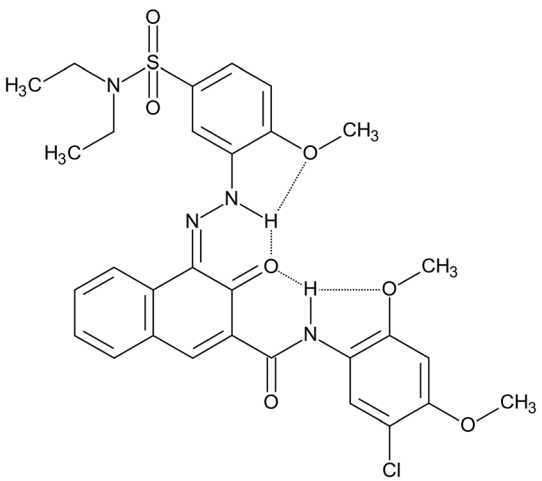

Scheme 1 Molecular formula of Pigment Red 5.

[a] *Institute of Inorganic and Analytical Chemistry, Goethe University, Max-von-Laue-Str. 7, 60438 Frankfurt am Main, Germany.*
E-mail: piepenbring@chemie.uni-frankfurt.de
[b] *Ernst Ruska-Center (ERC-1), Forschungszentrum Jülich, Wilhelm-Johnen-Straße, Jülich, 52428, Germany. E-mail: t.gorelik@fz-juelich.de*
[c] *Helmholtz Centre for Infection Research, Inhoffenstraße 7, 38124 Braunschweig, Germany*
[d] *Institute of Earth Sciences, Goethe University, Altenhöferallee 1, 60438 Frankfurt am Main, Germany*
† Former name: Martin U. Schmidt.

fastness (insolubility) is limited, *i.e.* paraffin wax or butter get red when coming in contact with prints containing P.R.5. The migration fastness is low, *i.e.* P.R.5 molecules tend to migrate within plastic, which hampers its use in PVC. The heat stability is low, as well, which impedes the use of P.R.5 in polymers such as PE or PP. The reason for these deficiencies is unknown, hitherto. Other hydrazone pigments with similar molecular formulae have better properties. Commercial grades of P.R.5 have a primary particle size of about 50–100 nm.

Pigments are insoluble in their application medium (*e.g.*, paint or printing ink). Consequently, they are not dissolved, but finely dispersed. Correspondingly, the crystal structure is maintained in the application medium, and the properties of the pigments, such as colour and photostability, depend on their crystal structures. Hence, the knowledge of their crystal structures is necessary to understand and tune the properties of the pigments by crystal engineering, *i.e.* by crystal modelling and by targeted synthesis of new chemical derivatives, new crystal phases or mixed crystals, which have desired crystal structures and properties.

Hydrazone pigments based on β-naphthol have been known since the second half of the 19th century. They have been industrially produced since about 1889.[3]

However, most β-naphthol pigments show some solubility in organic media, especially at elevated temperatures, which deteriorates their fastness properties such as solvent fastness, migration fastness in plastics, and temperature fastness. The properties are improved, if the solubility is reduced by the introduction of carbonamide groups leading to "naphthol AS" pigments, where "AS" stands for "Amid einer Säure" (in English: amide of an acid; it is the phenyl amide of 2-naphthoic acid), see Scheme 2. Their synthesis is shown in Scheme 3.

Pigments with even better properties are obtained, if additionally the phenyl ring of the diazo compound is substituted with carbon amide or sulfonamide groups. One of the first commercial pigments in this class was P.R.5, which was discovered by W. Nelmeier and W. Lamberg in Germany in 1931.[4] The first commercial product was "permanent carmine FB". Under a similar name ("Permanent Carmine FB01") the pigment is still produced today.

Despite decades of production and application, no crystal structure of P.R.5 had been available, leaving key structure–property links unresolved. Closing this gap is essential for rationalising P.R.5's fastness profile within the naphthol AS family.

One problem is its pronounced insolubility in water and all solvents, even at high temperatures, which hampers the growth of single crystals suitable for X-ray analysis.

In contrast, crystal structures are known for a series of other commercial naphthol AS pigments, including P.R.2,[5] P.R.170,[6,7] P.R.208,[8,9] P.R.266,[10] and Pigment Orange (P.O.) 22,[11] and several non-commercial pigments, *e.g.*, the chloro derivatives of P.R.9,[12] and Pigment Brown (P.Br.) 1.[13]

By analogy with related naphthol AS pigments, P.R.5 was expected to adopt the hydrazone form and layered π-stacking of the molecules, but its actual packing motif, intermolecular contacts and potential polymorphism remained unknown.

All crystal structure determinations revealed that the pigments do not adopt the originally assumed azo-tautomeric form (Scheme 2a), but instead consistently crystallise in the hydrazone-tautomeric form (Scheme 2b).[5–13] Consequently, these pigments are not "azo pigments" but should be classified as "hydrazone pigments".[3]

Several naphthol AS pigments are known to exhibit polymorphism; for example, P.R.170 has three documented polymorphs.[14] In contrast, no polymorphic forms of P.R.5 have been reported in the literature. The Powder Diffraction File[15] database also lists only a single phase—corresponding to the commercial form.

We conducted a polymorph screening of P.R.5, recorded powder diffraction patterns, and attempted to grow single crystals. However, in a long series of experiments, no crystals

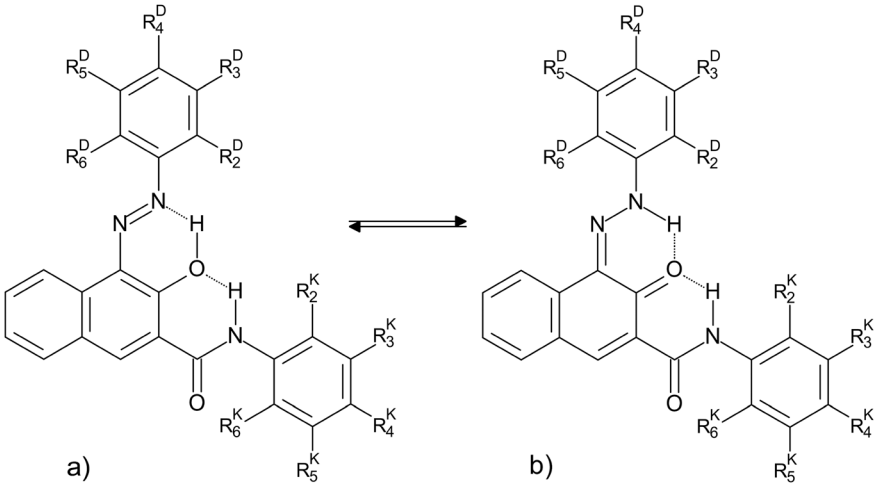

Scheme 2 Molecular formula of naphthol AS pigments. (a) Originally assumed azo tautomeric form. (b) Hydrazone form, which is actually adopted in the solid state.

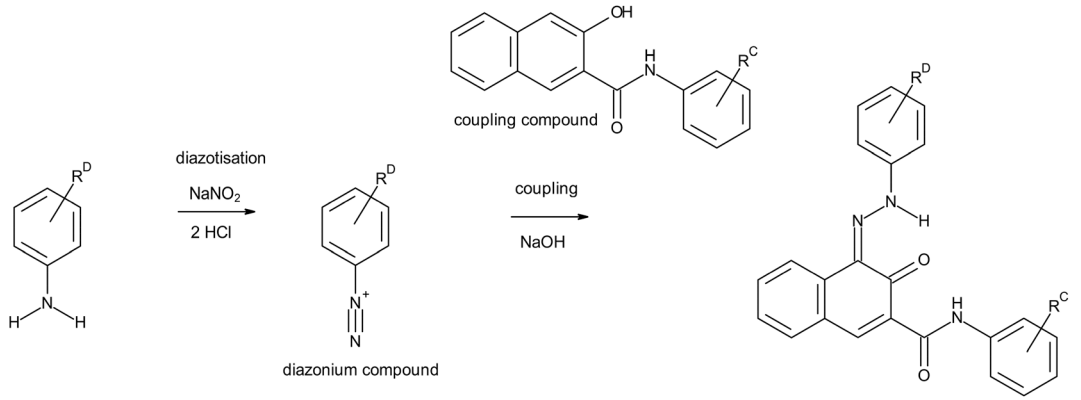

Scheme 3 Synthesis of naphthol AS pigments.

of sufficient size were obtained, and even all efforts to solve the structure from powder data were unsuccessful. Consequently, the crystal structure was determined using electron diffraction (ED).

Crystal structure determination of organic compounds by electron diffraction has evolved into a reliable and robust technique, resulting in nearly 500 new crystal structures determined from electron diffraction data and deposited into the CSD[16] to date. While diverse data acquisition techniques were proposed during the early stages of 3D electron diffraction (3D ED) development,[17] the majority of contemporary data are now collected using continuous rotation mode. Data reduction is typically performed using dedicated software for ED (such as PETS2),[18] or widely used software packages for processing X-ray single crystal diffraction data, such as XDS[19] and DIALS.[20] Successful structure determinations have been demonstrated across all data reduction routes.

Organic pigments represent classical candidates for 3D ED structure determination. They are notoriously poorly soluble, posing challenges for growing large crystals required for single crystal X-ray structure determination. Additionally, organic pigments often exhibit impurities or multiple polymorphs[3] and their crystallinity is frequently poor, complicating structure determination from powder X-ray data.[21] Moreover, their tendency toward low symmetry presents an inherent challenge for indexing powder diffraction data, where ED can support the analysis by delivering a reliable unit cell metric.[22,23]

All organic crystals are susceptible to electron beam damage, which poses challenges for data acquisition using electron diffraction. However, their resistance to radiation damage varies depending on their molecular composition and structural characteristics. Organic pigments often exhibit comparatively high stability under electron irradiation. This is likely due to their extended conjugated systems, which can delocalise energy, as well as their typically dense molecular packing and high lattice energies, which contribute to structural robustness.

The investigation of crystal structures of organic pigments by ED traces its origins back to the late 1970s.[24] A crystal structure of a hydrazone pigment was first determined by ED in 2009, using zone patterns.[22] Subsequently, with the introduction of 3D ED, numerous crystal structures of organic pigments have been elucidated. These include α^{II}-quinacridone (Pigment Violet 19),[25] copper perchlorophthalocyanine (Pigment Green 7),[24] as well as Pigment Orange 13,[26] and two distinct phases of pigment orange 34,[27] one of which is a high-temperature polymorph determined by ED at +220 °C.

Here we successfully applied 3D ED to determine the crystal structure of Pigment Red 5. Later, we obtained a small single crystal suitable for single crystal X-ray analysis, and the structure determined from this crystal matched the ED results. With the knowledge of the molecular packing, we applied crystal engineering. Based on the results of the crystal modelling, we synthesized derivatives and mixed crystals with improved properties.

2. Experimental

2.1 Materials

A commercial sample of Pigment Red 5 named "permanent carmine FB 01 M250" was obtained from Clariant (now Sudarshan, Frankfurt am Main, Germany). This sample was used without further purification as starting material for the polymorph screening and recrystallisation studies of P.R.5.

For the synthesis of P.R.5 and the mixed crystals 3-amino-*N*,*N*-diethyl-4-methoxybenzenesulfonamide (Fast Red ITR base) was obtained from Sigma-Aldrich. 5′-chloro-3-hydroxy-2′,4′-dimethoxy-2-naphthanilide (naphthol AS-ITR), 3-amino-4-methoxybenzanilide, and *N*-(4-chloro-2,5-dimethoxyphenyl)-3-hydroxy-2-naphthamide (naphthol AS-LC) were obtained from Heubach (now Sudarshan). All reagents were used as received without further purification.

2.2 Synthesis

2.2.1 Pigment Red 5. The synthetic procedure is based on the procedure given in ref. 28.

1.5 g of 3-amino-*N*,*N*-diethyl-4-methoxybenzenesulfonamide (Fast Red ITR base) was dissolved in 19 mL of water and 1.5 mL of concentrated hydrochloric acid. 0.401 g of sodium nitrite was added to the solution at 5 °C and stirred. After adding a spatula

of amidosulfonic acid, 1.4 g of sodium acetate was added. A second mixture of 2.1 g of 5′-chloro-3-hydroxy-2′,4′-dimethoxy-2-naphthanilide (naphthol AS-ITR), 1.23 g of NaOH, and 1600 mL of water (pH = 14) was slowly added dropwise to the first mixture. The suspension was heated to 80 °C for one hour and then filtered. The solid was dried at room temperature. Pigment Red 5 was obtained in almost quantitative yield as a nanocrystalline red powder.

To obtain a better crystalline powder, the dried red solid from synthesis or the commercial sample was suspended in boiling solvents, including water, ethanol, acetone, *p*-xylene, benzene, chlorobenzene, 1,2,4-trichlorobenzene and several more common solvents, for several hours. For details see 2.3.

2.2.2 Synthesis of mixed crystals. The mixed crystals were synthesized analogously to P.R.5, but using mixtures of diazo and/or coupling compounds:

a) A 3 : 1 mixture of Fast Red ITR base and 3-amino-4-methoxybenzanilide as diazo compounds, with naphthol AS-ITR as a coupling compound

b) A 1 : 1 mixture of Fast Red ITR base and 3-amino-4-methoxybenzanilide as diazo compounds, with naphthol AS-ITR as a coupling compound

c) A 3 : 1 mixture of Fast Red ITR base and 3-amino-4-methoxybenzanilide as diazo compounds, with a 3 : 1 mixture of naphthol AS-ITR and naphthol AS-LC as coupling compounds

d) 1 : 1 mixture of Fast Red ITR base and 3-amino-4-methoxybenzanilide as diazo compounds, with a mixture of 1 : 1 naphthol AS-ITR and naphthol AS-LC as coupling compounds

To obtain better crystalline powders, the resulting dried red solids were suspended in boiling solvents, including xylene, DMSO, nitrobenzene and 1,2,4-trichlorbenzene, for several hours.

2.3 Polymorph screening and recrystallization attempts

The commercial sample of P.R.5 was heated in a large variety of solvents including water, ethanol, cyclohexane, *n*-hexane, benzene, toluene, *p*-xylene, chlorobenzene, 1,2-dichlorobenzene, 1,2,4-trichlorobenzene, DMSO, *N*-methyl-pyrrolidone, and acetic acid. Most experiments were carried out at reflux temperatures. In total, about 30 experiments were performed. Melting and sublimation proved impossible; at very high temperatures (far above 300 °C), the compound decomposed.

The best powder pattern was achieved from a sample, which was obtained by heating a suspension of 0.375 g of P.R.5 in 50 mL chlorobenzene (b.p. 132 °C) to reflux for 3 hours. After cooling the suspension was centrifuged. The solvent was removed with a syringe, the remaining red powder was transferred into a glass vial using acetone, and the solvent was allowed to evaporate at ambient conditions.

2.3.1 Crystal growth. The best powder sample, obtained from a suspension in chlorobenzene, was used in the attempts for structure determination from powder data as well as for electron diffraction.

Eventually, tiny single crystals were obtained by heating a suspension of 0.039 g of P.R.5 in 50 mL 1,2,4-trichlorobenzene (b.p. 213 °C) to reflux for 4 hours. The suspension was cooled down slowly. 6 mL of the suspension were diluted with 40 mL 1,2,4-trichlorobenzene and heated to reflux for 5 hours. The seemingly clear fluid was cooled down slowly. The solvent was allowed to evaporate at 100 °C over 3 days, leading to tiny red needles. These needles were used for single crystal X-ray diffraction.

2.4 X-ray powder diffraction (XRPD)

Powder diffraction patterns were recorded using a Müller Mikro 111 diffractometer, which operated in reflection mode ($\theta/2\theta$) and was equipped with a copper fine-focus tube, a linear magazine, and a scintillation counter connected to a chart recorder. The generator settings were 40 kV and 30 mA. The chart recorder's paper speed was adjusted such that the resulting diffractograms exhibited a 2θ scale of 1.5° cm^{-1}. This procedure was used in the X-ray laboratory of Hoechst AG in Frankfurt-Höchst in 1979 for two samples prepared by Hoechst in 1997.

Powder patterns of all other samples were measured in transmission mode on a STOE Stadi-P diffractometer equipped with a Ge(111) monochromator using Cu-Kα_1 or Mo-Kα_1 radiation. The samples were prepared between polyacetate films. Two different detectors were used, a linear position-sensitive detector (PSD), and a Mythen 1K silicon strip detector. For the attempted structure determination from powder data the sample was prepared in a 1.0 mm capillary and carefully measured with a Mythen 1K silicon strip detector.

Attempts to index the powder pattern were made using DICVOL[29] implemented within the DASH[30] program. The obtained lattice parameters were tested using a Pawley fit in DASH. Structure solution trials were performed with the direct-space method using simulated annealing with the program DASH.

2.5 Electron diffraction

The powder sample obtained from chlorobenzene was dispersed in ethanol in an ultrasonic bath. A drop of the suspension was placed onto a holey carbon-coated copper TEM grid. The excess liquid was removed with filter paper. The grids were dried on air. The dry grids were clipped into grid-holding rings and transferred into a 200 kV Glacios transmission electron microscope (Thermo Fisher) at room temperature. The sample was cooled to liquid-nitrogen temperature within the TEM.

3D ED measurements were performed using the EPU-D (Thermo Fisher) module in continuous-rotation mode.[31,32]

Electron diffraction patterns were collected in nano-diffraction mode with the effective beam diameter on the sample of 1 μm. The tilt series were collected within −60⋯70° goniometer tilt range with 1° frame interval and a rotation speed of 0.5 s/1°. The data were collected using an electron dose rate of 6.016 e nm^{-2} s^{-1}. There was no evident crystal damage by electron beam.

Binning 4 of the CETA camera was applied, resulting in the effective pixel size of 0.002 $Å^{-1}$. The data were stored as MRC.

The MRC stacks were converted to TIFFs using a dedicated converter.[33] The data were analysed and reduced in *PETS2.*[18] 15 3D ED datasets were collected and processed, all delivering essentially the same unit cell. The 5 best datasets were used for structure determination. The crystal structure presented here was determined from one dataset only, showing the best performance. The original data are available at Zenodo (https://doi.org/10.5281/zenodo.19455732).

The structure was solved in SHELXD[34] and refined in SHELXL[35] within OLEX2 environment.[36] Non-hydrogen atoms were refined isotropically with AFIX constraints and SADI restraints, as anisotropic refinement led to non-positive definite thermal parameters. Hydrogen atoms were included in calculated positions.

Additionally a dynamical refinement was performed in JANA.[37]

2.6 Single crystal X-ray diffraction

A needle with a size of approximately 0.03 × 0.082 × 0.189 mm^3 was used for single-crystal X-ray analysis. Single-crystal X-ray diffraction was performed at 22 °C using an XCalibur3 four-circle diffractometer from Oxford diffraction equipped with graphite-monochromatized Mo-Kα radiation and a charge coupled device camera (Sapphire3). The samples were mounted on the goniometer head at a distance of 45 mm to the detector.

The diffraction data were processed using the Crysalis^{Pro} software from Rigaku, which facilitated indexing, data reduction, and empirical absorption correction. The structures were initially solved using ShelXT[38] and further refined with ShelXL[35] through the ShelXle graphical interface.[39] The refinement processes involved fitting the model to the observed diffraction data, optimizing parameters such as atomic positions and thermal vibrations to minimize the difference between the observed and calculated diffraction patterns.

The refinements of the crystal structures from single-crystal X-ray diffraction data involved full-matrix least-squares refinements with anisotropic displacement parameters applied to all non-hydrogen atoms. Hydrogen atoms were placed in calculated positions using standard geometric constraints (AFIX instructions), and were refined using the riding model. The hydrogen atom on the N–NH group, indicative of the hydrazone tautomeric form, was not observed directly in the Fourier difference map but was modelled based on interatomic distances between C, N and O atoms.

2.7 Crystal modelling

The procedure for the calculation of the voids is described in the SI.

Crystal modelling was performed with the program suite Materials Studio[40] (version 4.4) using the Forcite module.

For P.R.5, the cif file of the crystal structure determined by ED was used as a starting point for the lattice-energy minimisations. The experimental crystal symmetry ($P\bar{1}$, $Z = 2$) was maintained.

For the derivatives, the starting model was manually constructed on the basis of the crystal structure of P.R.5, *i.e.* assuming that the derivatives crystallise isotypically to P.R.5.

Additional lattice-energy minimisations were carried out on mixed crystals (solid solutions), again assuming that the mixed crystal is isotypically to P.R.5. Different ordered models with unit cells containing Pigment Red 5 and other derivatives were created by replacing the corresponding molecules in the crystal lattice of P.R.5. Compositions deviating from a 1 : 1 ratio were calculated with supercells of the sizes 2 × 1 × 1 (for a 3 : 1 composition, and a 1 : 1 : 1 : 1 quarternaly mixed crystal) and 2 × 2 × 2 (for a 9 : 3 : 3 : 1 composition). For all mixed-crystal calculations, the symmetry was set to *P*1.

The unit cells were quite large, especially for the quaternary systems with 9:3:3:1 composition, having more than 1000 symmetrically independent atoms per unit cell and unit cell volumes of more than 20 000 $Å^3$, which is at present too large for lattice-energy optimisations with DFT-D. Therefore, the lattice-energy were performed with force field methods.

The Dreiding force field[41] was employed in its Lennard–Jones (6–12) form. Atomic charges were derived by the Gasteiger[42] method. Ewald summation was used for Coulomb and van der Waals interactions. Three modifications were made in the Dreiding force field: for X–S–X bond angles (X = any atom) the α_0 parameter was set to 109.5° instead of 92.1°, in order to ensure a tetrahedral geometry for the C–SO_2–N fragment. Additionally the distance parameter for S_3–O_3 bonds was changed from 1.69 Å to 1.42 Å. For water molecules, the H–O–H bond angle parameter α_0 was set to 111.5°, which leads to a reliable crystal structure of ice.[43]

The Dreiding force field was developed to reproduce organic crystal structures at room temperature. Hence, average entropic effects are implicitly included in the van der Waals parameters.

The convergence criteria were set to "ultra fine".

For all systems, two calculations were carried out, one with fixed lattice parameters and one with free lattice parameters. The lattice energies given in this paper were derived from the calculations with free unit cell parameters, in order to reflect the distortion of the lattice upon the formation of mixed crystals. Lattice energies were calculated as the difference between the force-field energy of the crystal (including intramolecular energy terms) and the force field energy of a single molecule, which was calculated with the same force field in a large unit cell with cell parameters of 50 or 100 Å.

Lattice energies of physical mixtures were obtained by averaging the lattice energies of the corresponding pure compounds.

The formation of a solid solution is not only an enthalpic issue, but also an entropic one. Hence, we added an energy term for the mixing entropy: $E_{S,mix} = -T \times S_{mix}$. The mixing entropy S_{mix} is given by $S_{mix} = -R\sum_{i=1}^{k} x_i \ln(x_i)$, wherein x describes the molar fraction.

In order to estimate, if hydrates can be formed, the following reaction was investigated:

$$\text{Pigment} + n\text{H}_2\text{O} \rightarrow \text{Pigment}\,(\text{H}_2\text{O})_n$$

The lattice energy of the hydrate is calculated with the force field set-up described above. The value for liquid water was derived from the lattice energy of ice calculated with the same force field (−44.42 kJ mol^{-1})[44] the experimental fusion enthalpy of ice at 0 °C (6.01 kJ mol^{-1}) and the experimental enthalpy for heating water from 0 °C to 25 °C (1.88 kJ mol^{-1}).[45]

All energies are given in kJ mol^{-1} per molecule, for hydrates and solid solutions per pigment molecule.

3. Results and discussion

3.1 Polymorphism

Hitherto, only one polymorphic form of P.R.5 has been published. This form corresponds to the industrial product. The X-ray powder diffractogram of a commercial sample of P.R.5 (permanent red FB01 from Clariant) is shown in Fig. 1a. We call this phase "α-phase".

We performed a polymorph screening, starting from the commercial form. The pigment was treated in various ways, including heating suspensions of the pigment in water or solvents up to 213 °C. As far as visible, the pigment did not dissolve in any of these solvents, even using small amounts of pigment and large amounts of boiling solvents. Only by heating very small amounts of P.R.5 in very large amounts of boiling 1,2,4-trichlorobenzene at 213 °C, a clear solution could be obtained; but it cannot be ruled out that even this "solution" was actually a suspension of fine particles with sizes below 50 nm, which were too small to scatter the light and therefore remained invisible and resulted in a clear looking suspension. Attempts for melting and sublimation were to no avail.

For all samples obtained, we recorded the X-ray powder patterns. All powder patterns showed the same polymorphic form as the commercial sample.

From the archives of the former company Hoechst AG we know that a second polymorph of P.R.5 exists, which we call "β-phase" (see Fig. 1b). The corresponding experiments were carried out in the laboratory of Dr. Rieper in the pigments research group of Hoechst AG in 1979. Unfortunately, we do not know how this second phase was obtained.

Finally, we investigated the crude pigment emerging from synthesis: The synthesis was carried out in the usual way by diazotation and coupling in water, see Scheme 3. The resulting suspension of the pigment in water was heated to 80 °C for 1 hour; the pigment was isolated by filtration and dried at room temperature on air. The X-ray powder pattern showed the β-phase, see Fig. 2 (and Fig. S1 in the SI). Hence, P.R.5 has (at least) two polymorphs. The α-phase is the thermodynamically stable one at elevated temperature.

3.2 Crystal structure determination of the α-phase of Pigment Red 5

3.2.1 Attempts at structure determination from powder data. Among the various crystallisation attempts, the best powder pattern of the α-phase of P.R.5 was obtained from a sample heated in chlorobenzene for three hours. This sample was

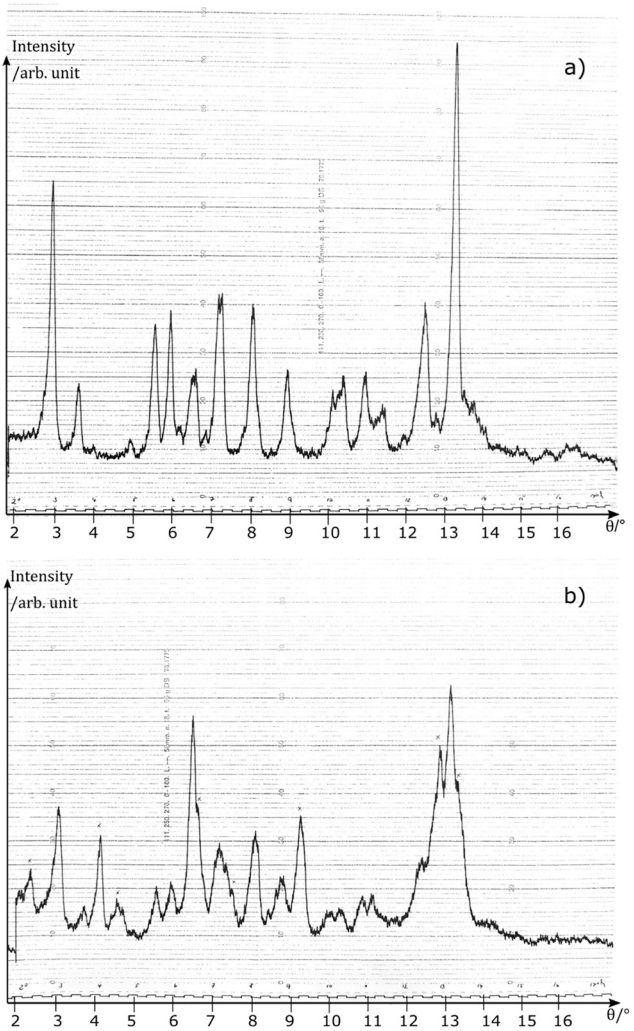

Fig. 1 X-ray powder patterns of P.R.5. (a) Commercial α-phase. (b) Mixture of the α-phase and the second phase (β-phase). These powder patterns were measured at Hoechst AG in 1979 using a chart recorder. Note: the horizontal axis is given in θ instead of 2θ.

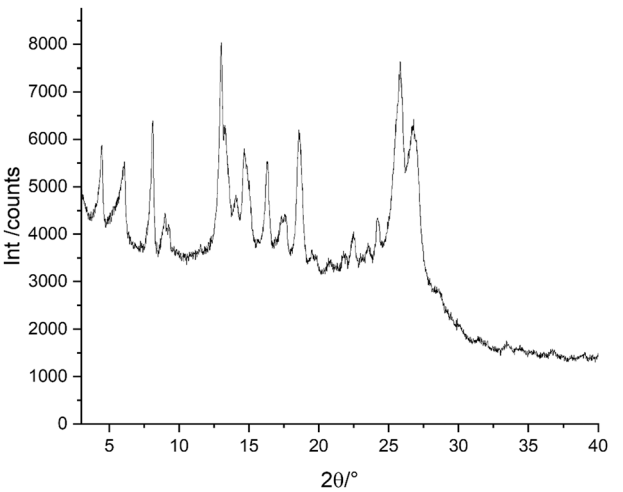

Fig. 2 X-ray powder pattern of the β-phase of P.R.5 obtained from synthesis.

remeasured over an extended 2θ range with an improved signal-to-noise ratio. To minimise preferred orientation, the sample was prepared in a capillary. The resulting pattern (Fig. 3b) exhibited numerous sharp reflections and appeared promising for structure determination from powder data.

However, indexing proved highly ambiguous. Several triclinic and monoclinic unit cells were proposed, but subsequent Pawley fits indicated that none were correct: either the fits were poor or some reflections remained unindexed. While unindexed reflections can, in principle, result from polymorphic mixtures or impurities, polymorph screening had confirmed that the P.R.5 powder was phase-pure and free of crystalline contaminants.

We then turned to electron diffraction (ED), initially aiming only to determine the lattice parameters. The resulting unit cell parameters were a = 7.40 Å, b = 13.83 Å, c = 16.43 Å, α = 66.77°, β = 89.55°, and γ = 75.04°. This set of parameters had not emerged in any of the previous indexing attempts. Based on the unit cell volume, it was clear that the cell contains two molecules. A subsequent Pawley fit converged with an excellent match, confirming the correctness of the lattice parameters obtained by ED.

The molecule of P.R.5 is achiral and lacks an inversion center. Therefore, the crystal symmetry was reasonably assumed to be $P\bar{1}$, with Z = 2 and Z' = 1, placing the molecule in a general position. We attempted to solve the structure from powder data using a direct-space approach with simulated annealing in the program DASH, as successfully done for many other organic pigments. However, in this case, the structure could not be solved, for reasons that remained unclear. Later we found out, that we had used an inadequate model for the molecular geometry.

Given the ease and promise of the preliminary electron diffraction (ED) experiments—and the compound's stability under the electron beam—we decided to determine the crystal structure by ED.

3.2.2 Structure determination of α-P.R.5 by electron diffraction. The TEM images showed that all crystals exhibited a plate-like morphology with a length-to-width ratio ranging from 2 : 1 to 3 : 1 (Fig. 4). The lateral size of the crystals was typically 2–3 μm. All crystals were oriented with their plate faces on the supporting carbon film. Most of the crystals were electron-transparent, indicating that they were sufficiently thin. From the TEM data, estimating the crystal thickness along the electron beam direction is highly challenging. These estimations typically rely on the expertise of electron crystallographers, who assess thickness based on the appearance of electron diffraction patterns, considering factors such as inelastic scattering background, the shape and intensity of Bragg reflections, and their contrast with the primary beam. The crystals of P.R.5 from chlorobenzene were relatively thin, likely between 200 and 300 nm in thickness.

From the 3D-ED data, a unit cell with triclinic metric was determined. No evidence of higher symmetry, diffuse scattering, or other anomalies were observed within the main crystallographic zones calculated as sections of reciprocal space (see Fig. 5).

All analysed crystals exhibited a similar orientation on the TEM grid, with their [001] crystallographic axis nearly aligned along the incident electron beam.

In total, 20 crystals were investigated by ED. Five datasets showed sufficient quality for a structure solution. For the structure determination we used the best-performing dataset and a merged dataset created from those five. The merging increased the completeness from 62.2 to 87.4%. The structure was solved using SHELXD.[34] Manual readjustments of atomic species (element types) were necessary for some atoms. Kinematical refinement using both datasets was performed in SHELXL[35] within the Olex2[36] environment. Hydrogen atoms were added in calculated positions using a riding model. During anisotropic refinement, several components of thermal factors turned negative, leading us to opt for isotropic refinement. AFIX 66 and SADI commands were applied

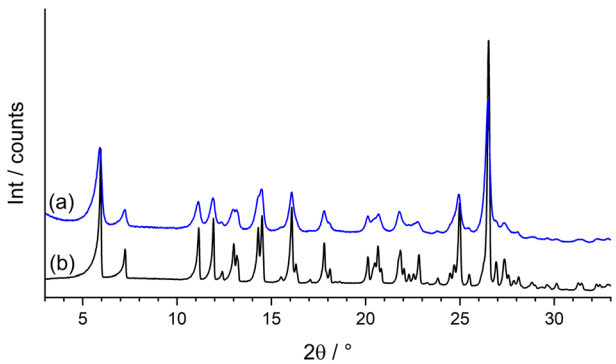

Fig. 3 X-ray powder patterns of P.R.5. (a) Commercial sample (permanent red FB 01 from Clariant). (b) Best powder pattern, obtained by heating the sample as a suspension in boiling chlorobenzene for three hours.

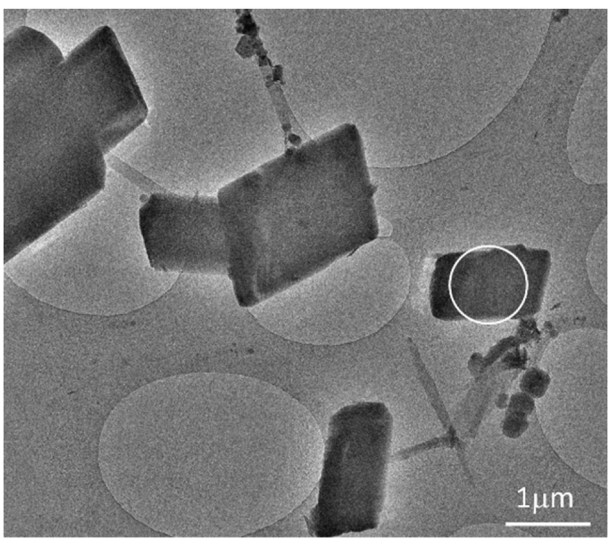

Fig. 4 TEM image of P.R.5 crystals used for ED measurements. The size of the electron beam used for ED data collection and its placement is marked by a white circle.

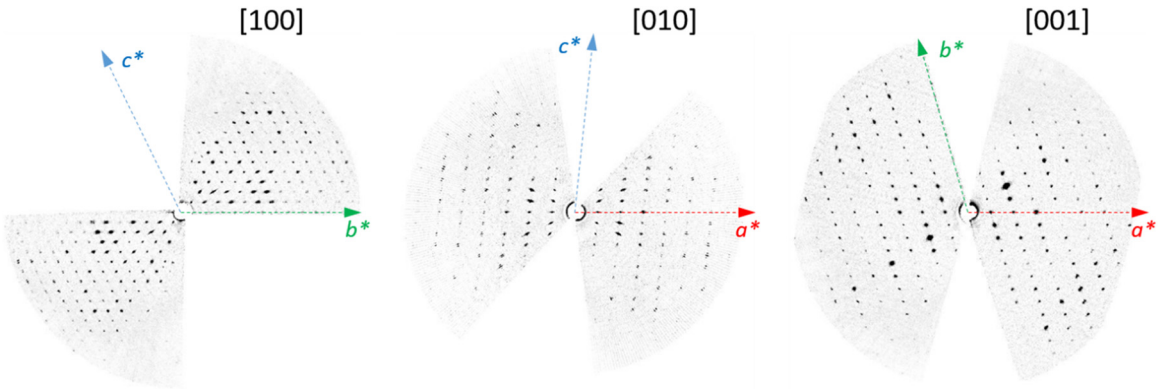

Fig. 5 Electron diffraction patterns. Crystallographic main zones calculated as section though the reciprocal space.

during the refinement. Merging of data improved the kinematical R factor from 30.95 to 22.44%. Additionally, dynamical refinement was performed in JANA[37] using the same best-performing dataset converging at 17.63%.

RMSDs for non-hydrogen atoms were calculated for the three structures. The RMSD between the kinematically refined structure from the single dataset (CSD 2545237) and that from the five-dataset merge (CSD 2544539) was 0.221 Å, and the RMSD between the kinematically refined (single dataset, CSD 2545237) and the dynamically refined structure (CSD 2498247) was 0.082 Å. These values indicate that the structures are essentially the same.

The final structure is shown in Fig. 6. The final difference Fourier map did not reveal any significant maxima (Fig. S4 in the SI). Crystallographic data are compiled in Table 1.

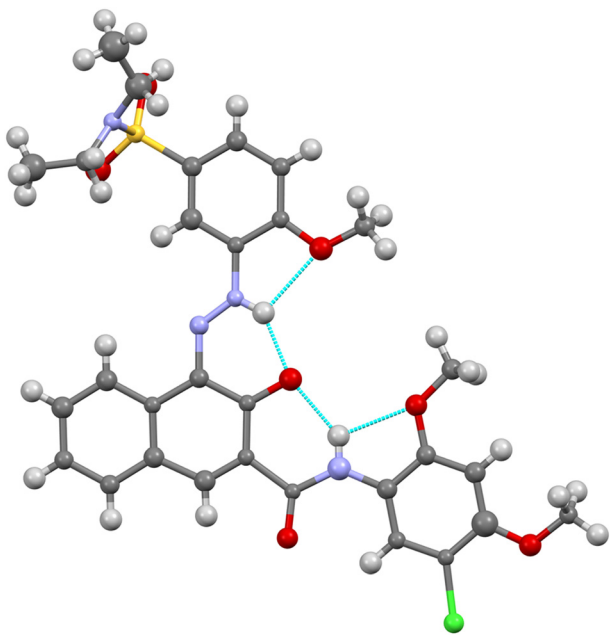

Fig. 6 Molecular structure of P.R.5 in the α-phase determined by electron diffraction. The size of the non-hydrogen atoms corresponds to the atomic displacement parameters at 50% probability (colour code: C grey, H white, N blue, O red, Cl green, S yellow).

3.2.3 Structure determination of α-P.R.5 by single crystal X-ray diffraction (SCXRD). Surprisingly, a later crystallisation experiment using boiling 1,2,4-trichlorbenzene with subsequent evaporation, yielded small single crystals in the form of thin needles, see Fig. 7a. Notably, these crystals were of a different morphology than the sample from chlorobenzene examined by electron diffraction. Whereas the crystals from chlorobenzene had the shape of parallelepipeds, the crystals from 1,2,4-trichlorobenzene were tiny, flat needles with a maximum length of 400 μm, see Fig. 7. For the X-ray diffraction experiment, we used a plate-shaped crystal with dimensions of approximately 0.03 × 0.082 × 0.189 mm^3. Although the crystal had a thickness of only 30 μm, it turned out to be suitable for single crystal X-ray analysis, using a laboratory diffractometer with a sealed X-ray tube.

Both turned out to be the same polymorph: the commercial α-phase of P.R.5. This was confirmed by comparing the experimental powder pattern of the α-phase with the simulated X-ray powder patterns derived from both the ED and SCXRD data (see Fig. S2 in the SI and Fig. S3 for an overlay of the structures).

The crystallographic data obtained by SCXRD are included in Table 1. The molecular structure and the anisotropic displacement parameters are shown in Fig. 8.

The SCXRD data nicely confirm the crystal structure determined by ED, despite the different crystal morphologies, and the different experimental conditions (SCXRD at 22 °C, *vs.* ED at −196 °C). Just the standard setting of the unit cell at room temperature (SCXRD data) is a different one than the standard setting at −196 °C (ED data).‡ In the following, we will use the −196 °C setting. A superposition of both structures is given in Fig. S3 in the SI. The SCXRD data also confirm the tautomeric form.

‡ The room temperature setting of the unit cell has to be transformed by (−1 0 0, −1 −1 0, 0 0 1) to obtain the −196 °C setting. To obtain the same set of fractional coordinates, subsequently the symmetry operation −*x*, −*y*, −*z* must be applied, and finally all atoms have to be translated by (0.5, 0.5, 1). The cif files contain the ED data.

Table 1 Crystallographic data of α-P.R.5, determined at −196 °C by ED (kinematical refinement of the best crystal), and at 22 °C by SCXRD. For the 22 °C data, two different unit cell settings are given. Cell setting I is the standard setting of the unit cell at −196 °C; cell setting II is the standard setting at 22 °C. In this paper, we use the cell setting I throughout

Compound	P.R.5	P.R.5	P.R.5	Mixed crystal of P.R.5 and Iso-P.R.5 (3)
Temperature/°C	−196	22	22	22
Data from	ED	SCXRD	SCXRD	SCXRD
Chemical formula	$C_{30}H_{31}ClN_4O_7S$	$C_{30}H_{31}ClN_4O_7S$	$C_{30}H_{31}ClN_4O_7S$	$C_{30}H_{31}ClN_4O_7S$[a]
Crystal data				
CCDC number	2 545 237	—	2 521 903	2 527 434
M_r	627.10	627.10	627.10	627.10
Crystal system	Triclinic Cell setting I	Triclinic Cell setting I	Triclinic Cell setting I[b]	Triclinic Cell setting II[b]
Space group (no.)	$P\bar{1}$ (2)	$P\bar{1}$ (2)	$P\bar{1}$ (2)	$P\bar{1}$ (2)
Z, Z'	2, 1	2, 1	2, 1	2, 1
a/Å	7.4362(8)	7.4665(6)	7.4665(6)	7.4867(5)
b/Å	13.839(3)	13.8307 (14)	13.8060(12)	13.8141(11)
c/Å	16.310(5)	16.2268(13)	16.2268(13)	16.0732(15)
α/°	65.85(2)	66.109 (9)	113.291(8)	113.141(8)
β/°	89.300(15)	88.906 (7)	91.094(7)	91.234(6)
γ/°	75.229(12)	74.144 (7)	105.492(7)	105.433(6)
V/Å^3	1472.92(7)	1465.8(2)	1465.8(2)	1458.5(2)
ρ_{calc}/g cm^{-3}	1.420(7)	1.421(5)	1.421 (5)	1.428 (5)
Radiation type	Electrons	X-rays, Mo K_α	X-rays, Mo K_α	X-rays, Mo K_α
Wavelength/Å	0.0251	0.71073	0.71073	0.71073
μ (mm^{-1})	—	0.257	0.257	0.258
Data collection				
Crystal size (mm)	0.003 × 0.002 × *ca.* 0.0003	0.191 × 0.088 × 0.030	0.191 × 0.088 × 0.030	0.04 × 0.10 × 0.11
Diffractometer	GLACIOS, EPU-D	Rigaku Xcalibur, Sapphire3	Rigaku Xcalibur, Sapphire3	Rigaku Xcalibur, Sapphire3
Specimen mounting	On a holey carbon-coated copper TEM grid	MicroLoops	MicroLoops	MicroLoops
Tilt range, increment, °	−60⋯70, 1	—	—	—
Data collection mode	Continuous rotation	Omega scans	Omega scans	Omega scans
$2\theta_{min}$/°	0.5322	5.134	5.134	5.176
$2\theta_{max}$/°	1.582	50.044	50.044	50.04
Refinement				
Completeness, %	62.2	99.7	99.7	99.8
Data resolution/Å	0.91	0.84	0.84	0.84
R_{int}	0.1381	0.1111	0.1111	0.0615
R_1 [$I \geq 2\sigma(I)$]	0.3095	0.0753	0.0753	0.1158
wR_2	0.6432	0.1190	0.1190	0.3402
gof	2.408	0.951	0.951	1.086
No. of reflections measured, unique reflections, thereof with with $I > 2\sigma(I)$	4114, 2560, 1683	19 850, 5171, 1979	19 850, 5171, 1979	20 534, 5151, 3504,
No. of refined parameters	143	393	393	508
No. of restraints	37	1	1	378
H-atom treatment	Riding model	Riding model	Riding model	Riding model
$\Delta\rho_{min}$, $\Delta\rho_{max}$	—	−0.271, 0.239	−0.271, 0.239	−0.401, 0.499

[a] The chemical formula is identical for both compounds. [b] This cell has to be transformed by (−1 0 0, −1 −1 0, 0 0 1) to obtain setting I. The cif file of the X-ray data contains the standard setting at room temperature, *i.e.* setting II.

3.3 Molecular structure and crystal structure of the α-phase of Pigment Red 5

The molecular structure of P.R.5 in the α-phase is shown in Fig. 6 and 8. The molecule is essentially planar, except for the SO_2NEt_2 fragment. The pigment adopts the hydrazone-tautomeric form, like all other naphthol AS pigments. The intramolecular hydrogen bonds follow the typical pattern of naphthol AS pigments with two bifurcated hydrogen bonds from the NH groups to the neighbouring oxygen atoms. There are no intermolecular hydrogen bonds.

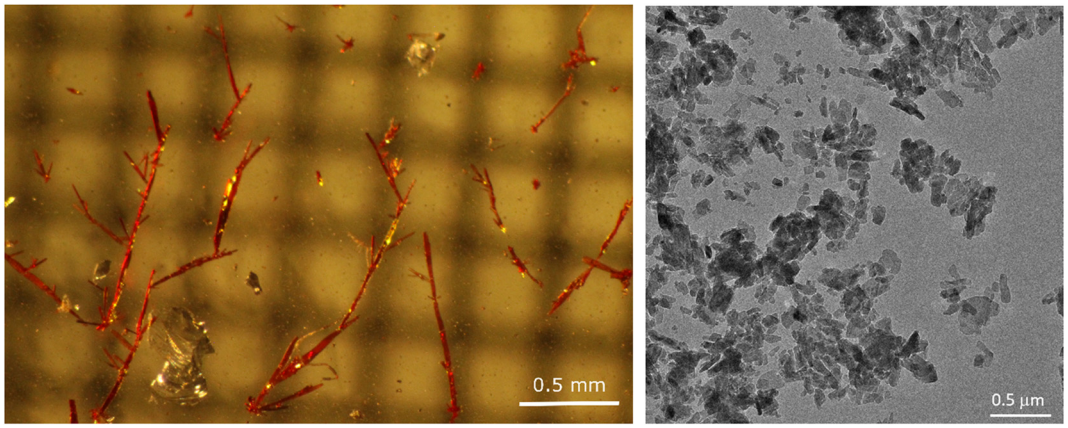

Fig. 7 Different morphologies of P.R.5 crystals. Left: needle-like crystals, obtained from 1,2,4-trichlorobenzene. Light-microscopic image. This sample was used for SCXRD. Right: commercial sample. All crystals correspond to the same polymorph (α-phase).

The molecules form stacks along the *a* direction. Within a stack, neighbouring molecules exhibit inverted orientations (see Fig. 9 and also Fig. S10 in the SI).

In lateral directions, the molecules form layers, see Fig. 10.

The molecules are connected in the *a* direction by π–π stacking, in the lateral directions by van der Waals interactions.

3.4 Morphology of α-P.R.5

As shown in Fig. 7, the crystals of the α-phase of P.R.5 exhibit different morphologies, depending on the conditions in synthesis, post-treatment and crystallisation: needles and platelets.

The sample from chlorobenzene demonstrated in the TEM quite uniform crystal morphology and size. All crystals had a parallelogram shape with angles of 105° and 75°, respectively (Fig. 4). The ratio of lateral dimensions ranged from 2 : 1 to 3 : 1, indicating that the crystals did not develop into needle-like structures.

For 11 electron diffraction datasets, we analysed the crystal orientation with respect to the crystallographic orientation matrix and observed that the direction of the longest crystal dimension corresponded to the *a* crystallographic axis, while the other lateral direction aligned with the *b* axis. Consequently, the angle between the crystal faces matched the *γ* angle of the unit cell (75.229(12)°), see Fig. S9 in the SI. The largest dimension of the crystal corresponds to the molecular stacking direction [100]. In this direction, the molecules have the strongest intermolecular interactions. In the third direction, *c*, the crystals are quite thin. Correspondingly, all analysed crystals lay with the (001) plane facing the supporting film. In [001] direction, the crystal growth is slow, because the molecules are held together only by (quite weak) van der Waals interaction between the ends of the molecules.

The crystal from 1,2,4-trichlorobenzene, investigated by SCXRD had a similar morphology. In cell setting I the main direction of growth is roughly parallel to the normal of the (110) face, which corresponds to the longest dimension of

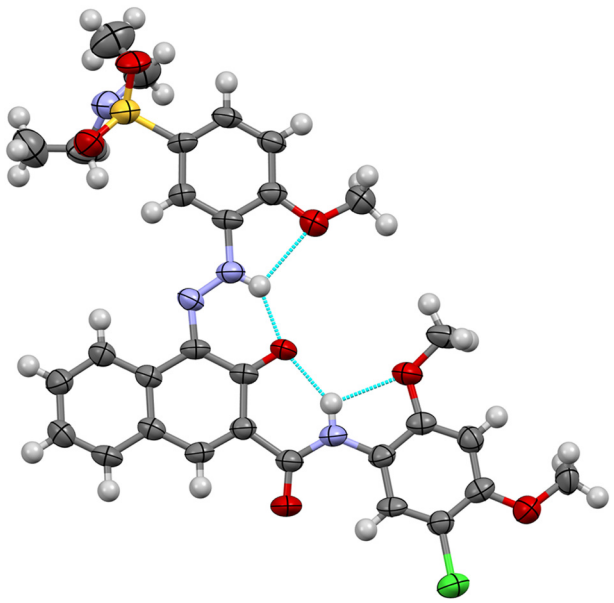

Fig. 8 Molecular structure of Pigment Red 5 at room temperature as determined by single-crystal X-ray diffraction. Ellipsoids are drawn with 50% probability.

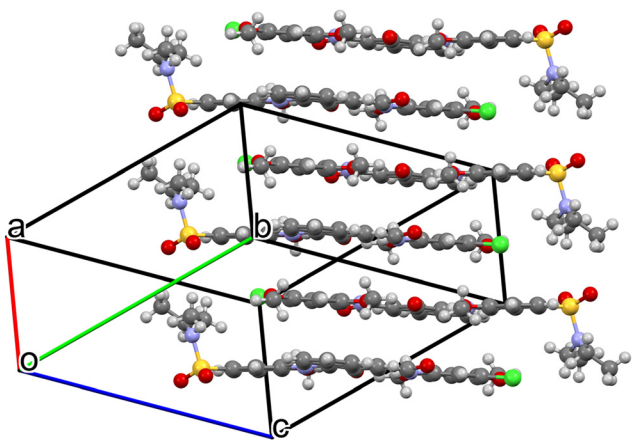

Fig. 9 Crystal structure of P.R.5. Stack of molecules parallel to [100]. ED data, view direction [3 −2 2].

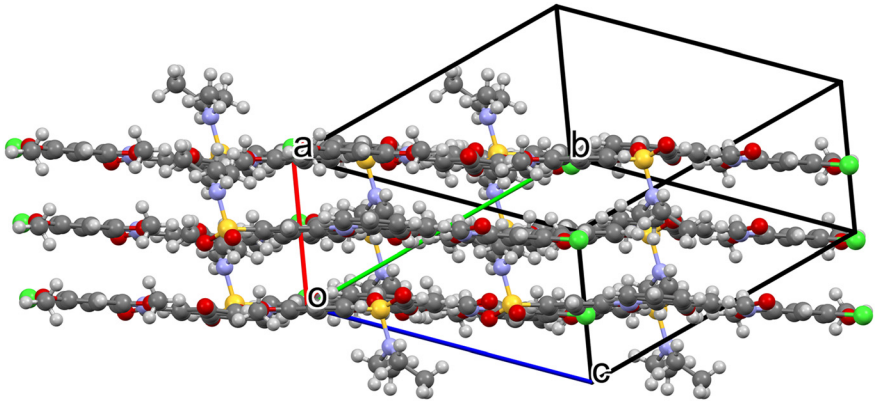

Fig. 10 Crystal structure of P.R.5. Layers of molecules parallel to [100]. ED data, view direction [3 −2 2].

the crystal of about 0.189 mm. The second most important direction of growth is roughly parallel to the normal of the (011) face resulting in a crystal width of about 0.082 mm. The thickness along the [001] direction is 0.030 mm.

The surface facets of the SCXRD crystal probably include {110}, {011} and {001}, although the exact assignment remains uncertain due to the small crystal size and the limited quality of the microscopic observation.

4. Crystal engineering on α-P.R.5

4.1 Molecular packing in organic pigments

All commercial organic pigments exhibit highly efficient and dense molecular packing. While typically organic compounds require, on average, a volume of 18 Å^3 per non-hydrogen atom,[46] this value drops to 16 Å^3 for many organic pigments, and even to 13 Å^3 for P.R.224 (perylenetetracarboxylic acid dianhydride). The same trend is observed using Detlef Hofmann's volume increment system,[47] which was fitted to the entire Cambridge Structural Database (CSD): on average, organic pigments are about 10% denser than organic compounds in general.

The efficient, dense molecular packing can be attributed to the functional requirements of commercial organic pigments. Over the past 120 years, industrial pigment research groups have synthesized tens of thousands of organic pigments and tested their application properties, yet fewer than 0.5% have made it into production. For an organic pigment to be commercially successful, it must exhibit excellent fastness properties—particularly solvent fastness (*i.e.*, insolubility), heat fastness (thermal stability, often above 300 °C), light fastness (photostability), and weather fastness (resistance to light, oxygen, and moisture). All these properties depend on strong stabilization of the molecules within the crystal lattice—that is, on high lattice energy and pronounced insolubility. Photostability, in particular, is closely linked to insolubility: molecules in solution are more easily destroyed by light, whereas a stable crystal lattice hampers photodecomposition reactions. Consequently, the best-performing organic pigments are those with the highest lattice energies and most efficient molecular packing. To date, no industrial organic pigments with voids in their crystal lattice have been reported.[3]

4.2 Voids in α-P.R.5

Astonishingly, the crystal structure of the commercial α-phase of P.R.5 displays a void between the SO_2NEt_2 groups of two neighbouring stacks (Fig. 11 and S8 in the SI).

The void is located on an inversion centre at (0.5, 0.5, 0). The position, shape and size of the void is essentially identical in both the structure obtained from electron diffraction at low temperature and the structure obtained from single crystal X-ray diffraction at room temperature. There is only one void per unit cell.

The void is surrounded by four ethyl groups, two SO_2 groups, two naphthalene fragments and two methyl groups of the methoxy fragment. The closest contact between the centre of the void and another atom is to a hydrogen atom of the naphthalene fragment (2.98 Å) and to an oxygen atom of the SO_2 group (3.20 Å).

This void has a size of about 36 Å^3 (36.4 Å^3 in the low-temperature structure obtained from ED, 37.8 Å^3 in the room-temperature structure obtained from X-ray diffraction). A water molecule would require a space of 22(8) Å^3, as determined by an extensive investigation of organic hydrate structures.[48] Correspondingly, the void would be large enough to host 1–2 water molecules, which would correspond to P.R.5 being a hemihydrate or a monohydrate. However, hydrates have never been observed for any crystal structure of a commercial Naphthol AS pigments despite many structural investigations. Also from our industrial experience, we never became aware of the existence of any hydrate of a commercial Naphthol AS pigment, and even not of any hydrate of any other commercial non-ionic organic pigment; the only exception are metal containing pigments (so called "laked pigments"), in which the metal ions are frequently coordinated by water molecules[3] – but P.R.5 contains no metal ions.

The void is empty. Our ED data show no significant electron density in the void (see Fig. S4 in the SI). In the X-ray data, the difference Fourier maps shows 4 peaks in the void with an electron density of only about 0.2 e Å^{-3}, which should be considered as noise, regarding the limited data quality.

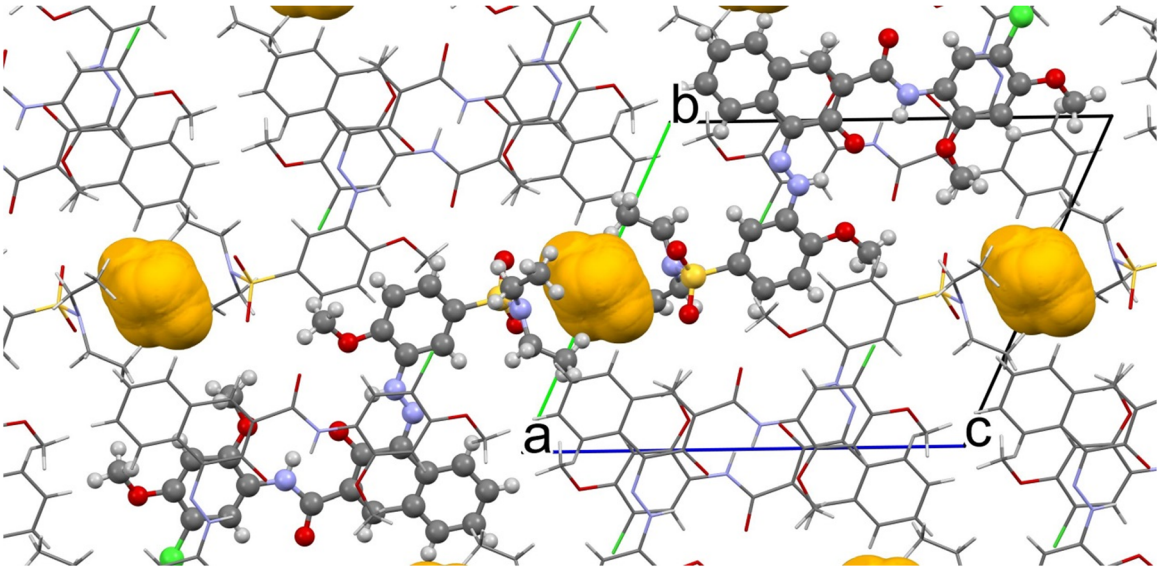

Fig. 11 Void (in yellow) between the SO_2NEt_2 groups in the crystal structure of α-P.R.5. The void represents the space, which is large enough to host a sphere with a diameter of 2.4 Å (which corresponds to the size of a water molecule). Details of the calculation method are given in the SI. Two molecules are highlighted. View direction [–100]. Data from ED (the SCXRD data give a similar picture, see Fig. S8 and S11 in the SI).

Hence, there are no water molecules in the void, and also no solvent molecules.

4.3 How could the voids be formed?

How are the voids formed? One possibility is that during synthesis—which is carried out in water—a hydrate initially forms. In the subsequent drying step, the water molecules may leave the crystal without significantly altering its structure.

During synthesis, the β-phase is initially formed. The α-phase emerges only after a post-treatment step (commonly referred to as "finishing"), in which the pigment is heated as a suspension in water or water-containing organic solvents.

It is theoretically possible that an intermediate "α-phase hydrate" initially forms during this process—an isostructural variant of the α-phase containing 1–2 water molecules within the voids. These water molecules could then be removed during the final drying step, leaving the overall arrangement of the pigment molecules largely unchanged. However, such hydrates have never been observed in any non-ionic commercial organic pigment.

Lattice-energy minimisations suggest that the incorporation of water would distort the crystal lattice of the α-phase, leading to significant changes in the positions and intensities of reflections in the X-ray powder pattern (see Fig. S12 in the SI). We carefully examined all our powder patterns for such deviations, but found no evidence of them: the patterns either matched the commercial, anhydrous α-phase or were too broad to allow definitive conclusions. However, some of the XRPD patterns showed very broad reflections, and, of course, we cannot rule out that these nanocrystalline or semi-amorphous materials could contain, at least partially, water in their crystal lattice.

All in all, there is no indication for a formation of voids *via* an intermediate hydrate. Instead, the compound appears to adopt a structure with intrinsic voids between the molecules—presumably because the molecular geometry prevents a more efficient packing.

4.4 Crystal engineering: filling the voids in α-P.R.5

4.4.1 Concepts. The application properties of P.R.5 are not as good as of some other naphthol AS pigments. For example, the solvent fastness of P.R.5 is worse than of P.R.170 (Scheme 2, R_4^D = $CONH_2$, R_2^K = OEt), although the molecule of P.R.170 is smaller.

We assume that the mediocre properties of P.R.5 are (at least, partially) caused by the void in the crystal structure of

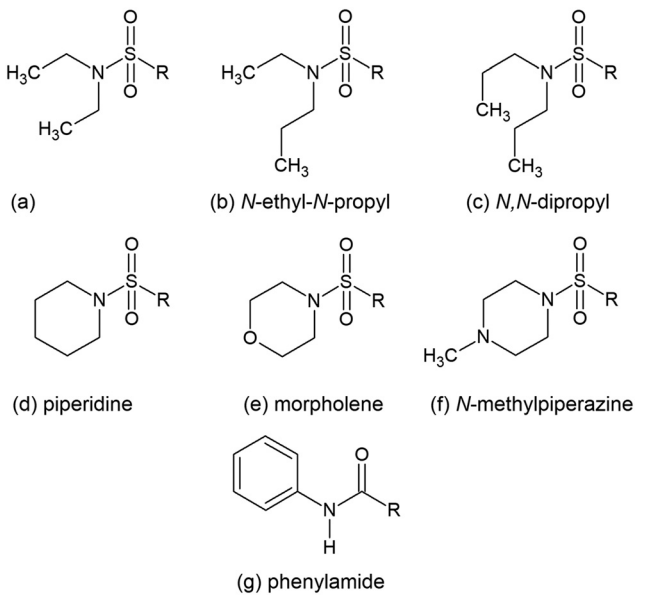

Scheme 4 Replacing the SO_2NEt_2 group of P.R.5 (a) with a slightly larger fragment (b–g). R indicates the rest of the P.R.5 molecule.

P.R.5. Filling the void would lead to a more efficient molecular packing, which increases the lattice energy and leads to a more stable crystal with improved fastness properties.

There are various possibilities to fill this void, including

- Replacing the NEt_2 group by a slightly larger fragment, such as NEtPr (Pr = *n*-propyl), NPr_2, piperidine, morpholine or *N*-methylpiperazine, see Scheme 4b–f.

- Replacing the entire SO_2NEt_2 group by a CO–NH–Ph (phenylamide) group (Scheme 4g).

In either case the new substituent has to be small enough to not disturb the crystal structure of P.R.5.

In contrast to the possibly void filling substituents, replacing the NEt_2 group by a smaller $N(CH_3)_2$ group would even increase the size of the void (or lead to a completely different crystal structure). Correspondingly, the $N(CH_3)_2$ derivative of P.R.5 is not industrially produced.

Filling the void with the groups b–g leads to new derivatives. These new derivatives could either adopt the same crystal structure as P.R.5, resulting in a similar shade but (hopefully) improved light fastness, or in a crystal structure with a fully different molecular arrangement, with probably a less interesting colour shade and unpredictable light fastness.

The chance to maintain the molecular arrangement of P.R.5 is increased by synthesising a solid solution (mixed crystal) of P.R.5 with one of the new derivatives.

In pigment science and industry, mixed crystals (solid solutions) are a common way to stabilize polymorphic forms and/or to tune the pigments' properties.[3,6,49,50] In most cases, the mixed crystal components are similar in size, shape and hydrogen bond abilities, so that, a solid solution is formed, *i.e.* the individual molecules are statistically distributed over the positions in the crystal.

The phenylamide group is also found in a similar Naphthol AS pigment, Pigment Red 146, Scheme 5. Note that P.R.146 differs from P.R.5 additionally in the exchange of OCH_3 and Cl substituents in the naphthol AS fragment. The crystal structure of P.R.146 is not published, hitherto. Yet, we were especially curious to investigate, if a solid solution of the four-component system of P.R.5, P.R.146 and the two mixed derivatives **2** and **3** could be obtained (Scheme 5).

4.4.2 Crystal modelling. Crystal modelling was applied to study the feasibility of various solid solution systems prior to experimental synthesis. This approach allowed a systematic preselection of potentially successful candidates based on structural compatibility.

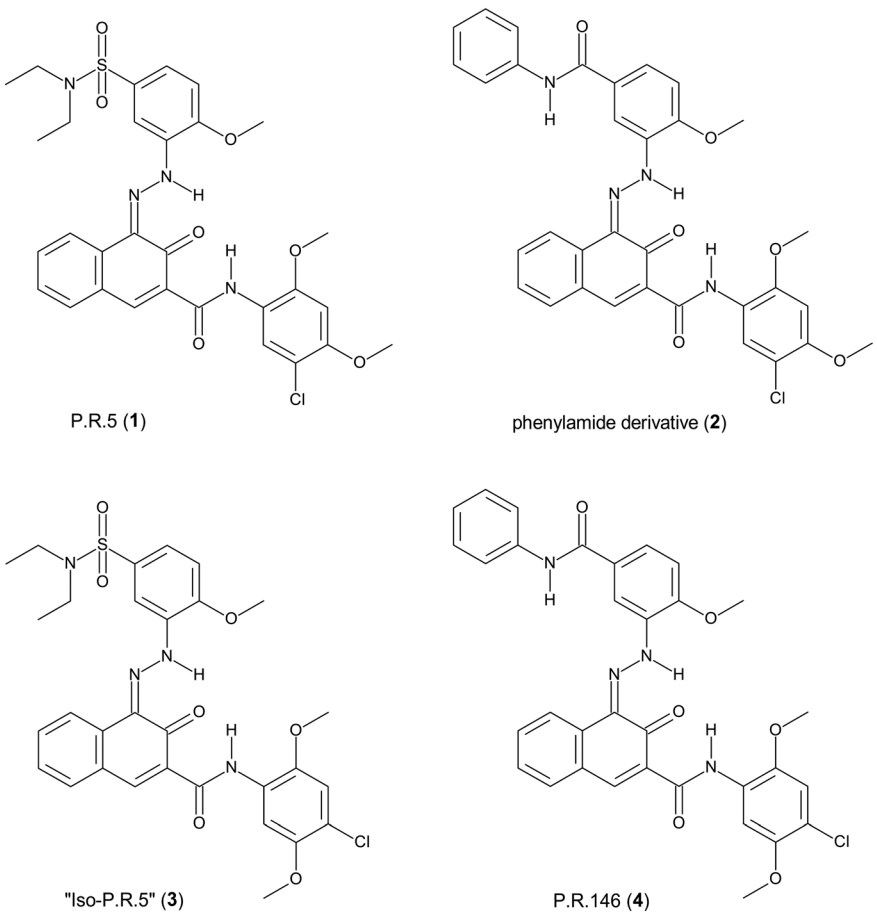

Scheme 5 Different possible compounds in the synthesized solid solutions.

Table 2 Lattice energies of P.R.5, its hypothetical hydrates and different solid solutions (mixed crystals) determined by crystal modelling. All listed calculations were performed with free lattice parameters. For the 1 : 1 mixed crystal of P.R.5 with its phenylamide derivative, two different structures were calculated, see text

Compound	Molar ratio P.R.5: derivative	Lattice energy of the mixed crystal H/kJ mol^{-1}	Lattice energy of the physical mixture H/kJ mol^{-1}	Difference between the lattice energy of the mixed crystal and of the physical mixture ΔH/kJ mol^{-1}	Mixing entropy S_{mix}/kJ mol^{-1} K^{-1}	Energy difference including the mixing entropy ΔE/kJ mol^{-1}
P.R.5	—	−258.78	—	—		
P.R.5*0.5H_2O	—	−263.81	—	13.24		
P.R.5*H_2O	—	−273.90	—	21.38		
P.R.5 + phenylamide derivative (**2**)	3 : 1	−244.75	−254.17	9.418	0.005	7.93
P.R.5 + phenylamide derivative (**2**) structure A	1 : 1	−247.82	−249.57	1.74	0.006	−0.04
P.R.5 + phenylamide derivative (**2**) structure B	1 : 1	−248.82	−249.57	0.74	0.006	−1.04
1 + **2** + **3** + **4**	1 : 1 : 1 : 1	−239.32	−255.04	15.72	0.012	12.14
1 + **2** + **3** + **4**	9 : 3 : 3 : 1	−247.58	−256.03	8.45	0.013	4.57
P.R.5 + *N*-ethyl-*N*-propyl derivative	1 : 1	−220.64	−245.86	25.23	0.006	23.43
P.R.5 + *N*,*N*-dipropyl derivative	1 : 1	−248.31	−262.91	14.60	0.006	12.81
P.R.5 + piperidine derivative	1 : 1	−231.32	−250.94	19.61	0.006	17.83
P.R.5 + morpholine derivative	1 : 1	−242.54	−248.12	5.58	0.006	3.79
P.R.5 + *N*-methylpiperazine derivative	1 : 1	−257.95	−263.76	5.81	0.006	4.02

A series of molecular derivatives of slightly larger size than P.R.5 (already discussed in 4.4.1) were selected and analysed with the aim of achieving a denser crystal packing. We assumed, that a slight increase in molecular volume might lead to a more efficient space filling, and thereby enhancement of the lattice stability, without a drastic change to the crystal structure.

Additionally we investigated the hypothesis of potential water molecules filling the void at some point during the synthesis of the pigment, by inserting one or two water molecules in the void, corresponding to a hemihydrate or monohydrate. Lattice-energy minimisation revealed that this insertion leads to an increase of the lattice energy, marking the inclusion of water in the structure as unfavourable. Furthermore, the inclusion of water into the anhydrous structure led in both cases to a distortion of the crystal lattice, which could not be observed experimentally in any of the powder patterns (see above). All in all the occurrence of a hydrate is very unlikely.

The calculations of the binary solid solution were carried out with a 1 : 1 or 3 : 1 ratio of P.R.5 and the corresponding derivative. The quaternary solid solution **1** + **2** + **3** + **4** was calculated with a ratio of 1 : 1 : 1 : 1 and 9 : 3 : 3 : 1 (corresponding to a 3 : 1 mixture of diazo compounds and a 3 : 1 mixture of coupling compounds).

For the 1 : 1 mixed crystal of P.R.5 and the phenylamide derivative, two structures were investigated:

A) A unit cell with one molecule of each compound. In this structure, each void is surrounded by one SO_2NEt_2 and one CONHPh group.

B) A unit cell with $a' = 2a$ containing a pair of P.R.5 molecules and a pair of phenylamide derivatives, so that half of the voids is empty whereas the other half is filled with two phenylamide groups.

An overview on the results is given in Tables 2 and 3.

For pure P.R.5, the geometry optimization starting from the experimentally determined crystal structure of the α-phase led to a closure of the void, primarily due to a rotation of the NEt_2 group. Probably this effect is an artefact caused by the force field.

The best energy for the formation of a mixed crystal was found for the 1 : 1 mixed crystal of P.R.5 with the phenylamide derivative **2**. For this system, the calculated lattice enthalpy of the mixed crystal (solid solution) is still slightly worse than that of the physical mixture, but due to the mixing entropy, the final energy of the mixed crystal is slightly better than for a physical mixture. Hence this mixed crystal should form.

In contrast, the solid solutions of P.R.5 with only 25% of **2**, is energetically unfavourable. Also a quaternary mixed crystals of **1** + **2** + **3** + **4** is calculated to be unfavourable.

Mixed crystals with other derivatives led as well to a pronounced increase (*i.e.* deterioration) of the lattice energy, indicating that these mixed crystals are difficult or impossible to obtain.

Astonishingly, the mixed crystal of P.R.5 with the *N*-ethyl-*N*-propyl derivative is calculated to be energetically less favourable

Table 3 Cell parameters of the modelled mixed crystals

	a/Å	*b*/Å	*c*/Å	*α*/°	*β*/°	*γ*/°
P.R.5*0.5H_2O	7.6009	14.1347	17.0595	62.7385	88.1784	76.9876
P.R.5*H_2O	7.9149	14.1022	17.2411	59.4359	85.2504	76.1075
P.R.5 + phenylamide derivative (**2**), 3 : 1	15.0933	14.0347	17.2324	63.3110	89.0344	77.0559
P.R.5 + phenylamide derivative (**2**), 1 : 1 structure A	12.0521	14.8204	17.8535	77.8666	39.4841	57.8351
P.R.5 + phenylamide derivative (**2**), 1 : 1 structure B	15.3067	12.1801	17.8651	79.4216	101.8188	84.1726
1 + **2** + **3** + **4**, 1 : 1 : 1 : 1	14.7823	13.7832	17.7597	65.0730	90.9970	79.7544
1 + **2** + **3** + **4**, 9 : 3 : 3 : 1	14.4300	30.9737	35.2079	62.7259	79.7686	64.2876
Phenylamide derivative (**2**)	8.3657	14.8714	14.7658	77.3096	83.1981	62.3703
P.R.5 + *N*-ethyl-*N*-propyl derivative, 1 : 1	7.6000	14.4735	18.5824	75.3483	108.8969	70.2904
P.R.5 + *N*,*N*-dipropyl derivative, 1 : 1	9.7723	20.0998	17.9455	56.8590	50.5296	38.0060
P.R.5 + piperidine derivative, 1 : 1	7.7200	12.6516	19.2922	83.2406	117.5060	82.8820
P.R.5 + morpholine derivative, 1 : 1	7.4593	14.9191	17.1640	64.2690	83.1261	66.9369
P.R.5 + *N*-methylpiperazine derivative, 1 : 1	11.0263	18.5684	18.0288	49.9044	38.8425	49.1679

than that with the *N*,*N*-dipropyl derivative, although the *N*-ethyl-*N*-propyl derivative is sterically less demanding. It is likely, that this result is an artefact, *i.e.* that the obtained *N*-ethyl-*N*-propyl structure does not correspond to the optimal molecular arrangement, but to a local energy minimum.

The piperidine derivative as well shows a pronounced increase in its lattice energy. In contrast, the mixed crystals with the *N*,*N*-dipropyl, the morpholine and the *N*-methylpiperazine derivatives display lattice energies to only slightly larger than the comparative physical mixtures.

Simulated powder patterns of the solid solutions are shown in the SI, Fig. S13 and S14.

Fig. 12–14 present a selection of the calculated crystal structures; further examples are provided in the SI (Fig. S15–S18).

Experimental investigations with the phenylamide derivative were subsequently carried out, as in the modelling studies only these solid solutions appeared to be promising.

4.4.3 Synthesis of mixed crystals. Mixed crystals (solid solution) of P.R.5 and the corresponding derivatives were synthesized by mixing the corresponding amines. This mixture was diazotated and coupled with the corresponding naphthol AS derivative.

Mixed crystals were synthesized with 75% of P.R.5 and 25% of the phenylamide derivative (**2**). After a finish (heating in suspension) in DMSO, the X-ray powder pattern nicely showed that a mixed crystals is formed, which is isostructural to the α-phase of P.R.5, see Fig. 15a. However the shifts of the peak positions (both towards higher and lower 2*θ* values) are very small, so there is only a slight change in the lattice parameters from P.R.5 to the mixed crystal. Finishing in nitrobenzene led to a mixture of two phases, one containing a mixed crystal isostructural to α-P.R.5, the structure of the other phase is unknown so far, but its powder pattern shows some slight similarities to the powder pattern of P.R.146.

A cosynthesis of 50% of P.R.5 and 50% of (**2**) with a subsequent finish in 1,2,4-trichlorobenzene led to a phase mixture of a mixed crystal isostructural to α-P.R.5, and a phase of unknown structure and composition (see Fig. S19).

We also synthesized a mixed crystal using a mixture of two diazonium components (the ones of P.R.5, and P.R.146) and a mixture of two coupling components (the ones of P.R.5 and P.R.146) in a ratio of 3 : 1 each, leading to a mixture of four components: P.R.5, the derivative (**2**), the corresponding derivative (**3**) with the coupling component of P.R.146, and P.R.146 (**4**) itself, in a presumable ratio of 9 : 3 : 3 : 1. After trichlorobenzene finish, the X-ray powder pattern revealed, that—as desired—a mixed crystal was formed. However a second phase is present as well. Due to the different size and shape of the four molecules, the lattice is considerably distorted, see Fig. 16.

The same experiment was performed using the starting materials in a ratio of 1 : 1, leading to a four-component mixture in a ratio of 1 : 1 : 1 : 1. With a DMSO finish, a mixed crystal isostructural to P.R.5 was obtained (Fig. 17a). When using xylene, toluene or trichlorobenzene as finishing solvents, a mixture of the two solid solution discussed before was observed: one isostructural to P.R.5 and one showing a powder pattern similar to P.R.146 (Fig. 17b). Interestingly, after a finish in nitrobenzene, the precipitate showed only the mixed crystal phase potentially isostructural to P.R.146 (Fig. 17c). However, after allowing the filtrate to slowly evaporate, small crystals of the mixed crystal phase isostructural to P.R.5 were obtained (Fig. 17d). This indicates a significant difference in solubility between the two mixed crystal phases in nitrobenzene. These single crystals show the most visible distortion of the lattice parameters, we observed during the experiments (see Fig. 17).

The crystal structure of the small crystals was determined with single crystal X-ray analysis.

4.4.4 Structure determination of the mixed crystal. The obtained small crystals from a 4-component synthesis of **1** + **2** + **3** + **4** in a 1 : 1 : 1 : 1 ratio (Fig. 18) were investigated by single crystal X-ray analysis.

To our surprise, the crystals only contained two of the expected compounds: P.R.5 and its isomeric derivative **3**, in which the Cl and OCH_3 group are exchanged (Fig. 19).

According to the atomic occupancies, these two compounds are present in 7 : 3 ratio. The residual electron density gave no indication of a presence of a replacement of SO_2NEt_2 by phenylamide groups. The lack of indication of the phenylamide derivatives **2** and **4** is presumably due to the

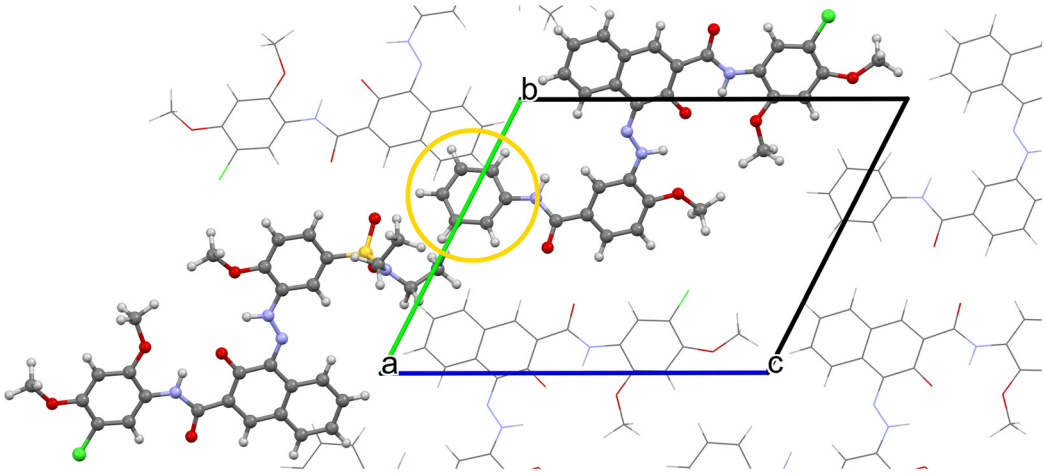

Fig. 12 Modelled crystal structure for a mixed crystal containing P.R.5 and the phenylamide derivative in a 3 : 1 ratio (coloured by atom type). The phenylamide group, which fills the void, is marked with a yellow circle.

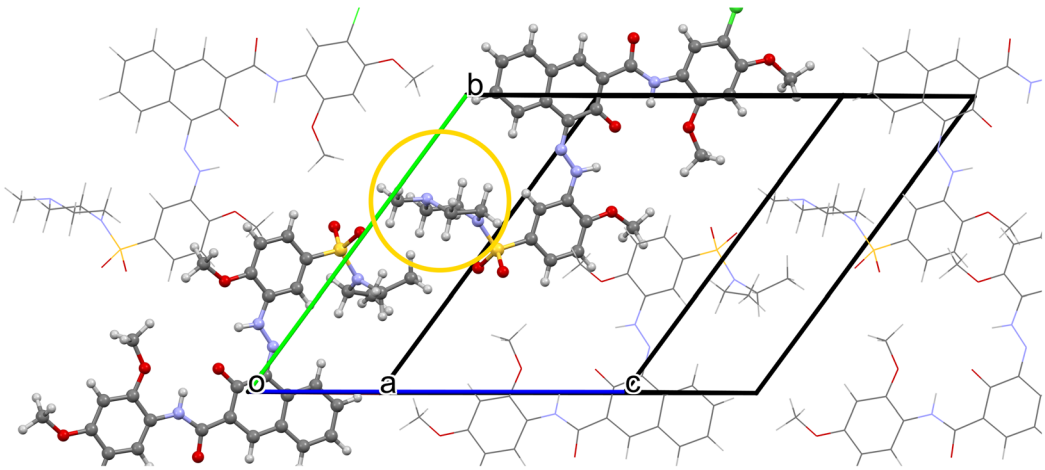

Fig. 13 Modelled crystal structure for a mixed crystal containing P.R.5 and the *N*-methylpiperazine derivative in a 1 : 1 ratio (shown coloured by atom type). The piperazine group filling the void is marked with a yellow circle.

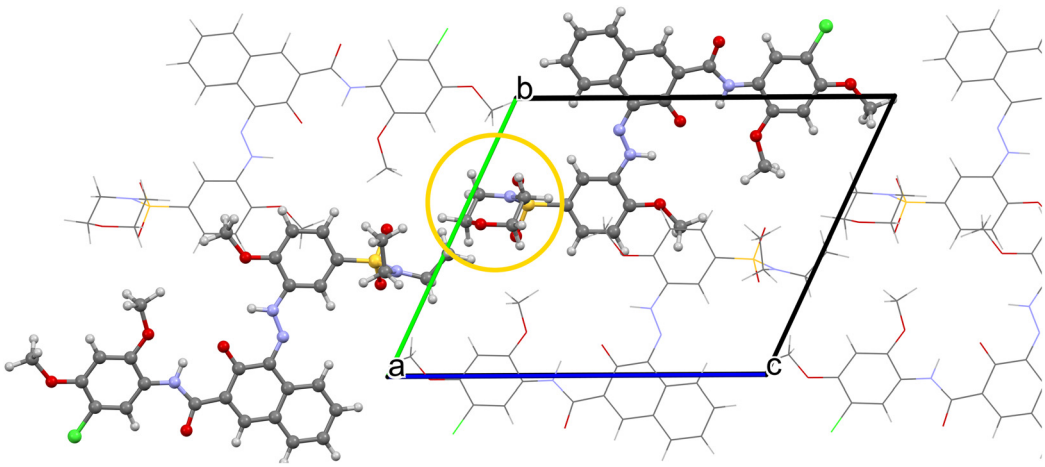

Fig. 14 Modelled crystal structure for a mixed crystal containing P.R.5 and the morpholine derivative in a 1 : 1 ratio (shown coloured by atom type). The morpholine group filling the void is marked with a yellow circle.

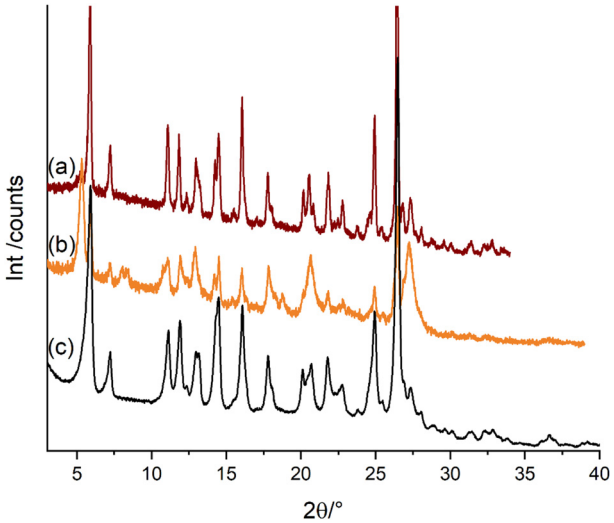

Fig. 15 Formation of a mixed crystal of P.R.5 and the corresponding phenylamide derivative in a ratio of 3 : 1. a) Powder data of the mixed crystal prepared by DMSO finish. b) Powder data of the mixed crystal prepared by nitrobenzene finish, showing a mixture with a second phase. c) Powder data of the commercial sample of P.R.5.

fact that P.R.146, and possibly also **2**, exhibit even lower solubility and therefore precipitate prior to crystallization or dissolve to a lesser extent during the heating process in the solvent. The disorder of OCH_3 and Cl groups only induces a slight distortion of the lattice. In contrast to our intended objective, the formation of the solid solution did not affect the void, as the crystal structure remains intact and the modification occurs at the wrong position of the molecule.

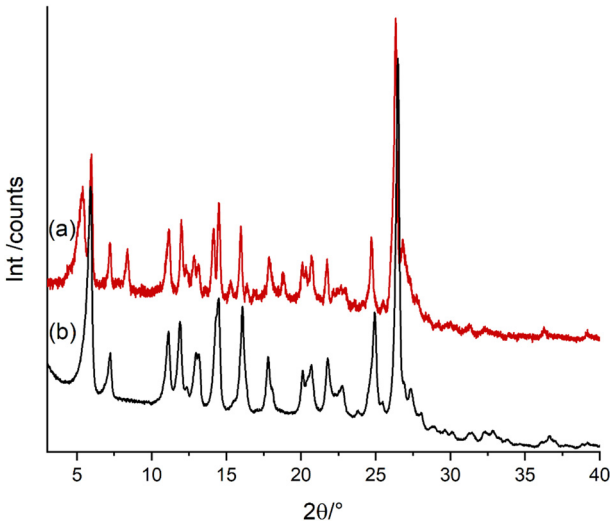

Fig. 16 Formation of a mixed crystal of P.R.5 and the corresponding phenylamide derivative, as well as the two corresponding coupling components, each in a ratio of 3 : 1. a) Powder data of the mixed crystal prepared by trichlorobenzene finish (phase mixture). b) Powder data of the commercial sample of P.R.5.

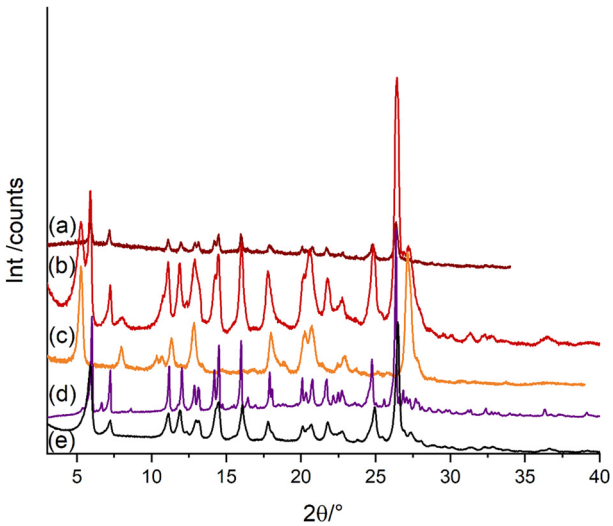

Fig. 17 X-ray powder diffractograms showing the formation mixed crystals with P.R.5 (synthesis with all four components in a 1 : 1 : 1 : 1 ratio). a) Solid solution heated in DMSO after the synthesis. b) Solid solution heated in trichlorobenzene after synthesis. c) Solid solution heated in nitrobenzene after synthesis (fresh sample). d) Powder data of single crystals of the P.R.5 solid solution grown from nitrobenzene filtrate, ground to powder. e) Commercial sample of P.R.5 (α-phase).

4.4.5 Results of the crystal engineering on P.R.5. The powder patterns confirm the successful synthesis of several different mixed crystals. The observed peak shifts in the diffractograms indicate variations in the composition of these solid solutions, reflecting different degrees of incorporation of the derivatives into the crystal lattice of P.R.5.

According to lattice-energy calculations, a mixed crystal of P.R.5 containing 25% of the phenylamide derivative **2** should not be accessible, because it is energetically less favourable than a physical mixture of the individual compounds. Nevertheless, we could synthesise such a mixed crystal, as proven by XRPD. The same disagreement was found for mixed crystals of **1** + **2** + **3** + **4**. Also here, the mixed crystal could be

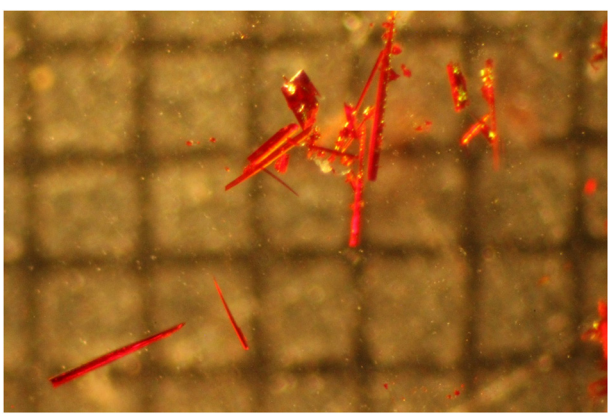

Fig. 18 Crystals of the solid solution of **1** and **3** used for single X-ray analysis. 0.5 mm grid in the background.

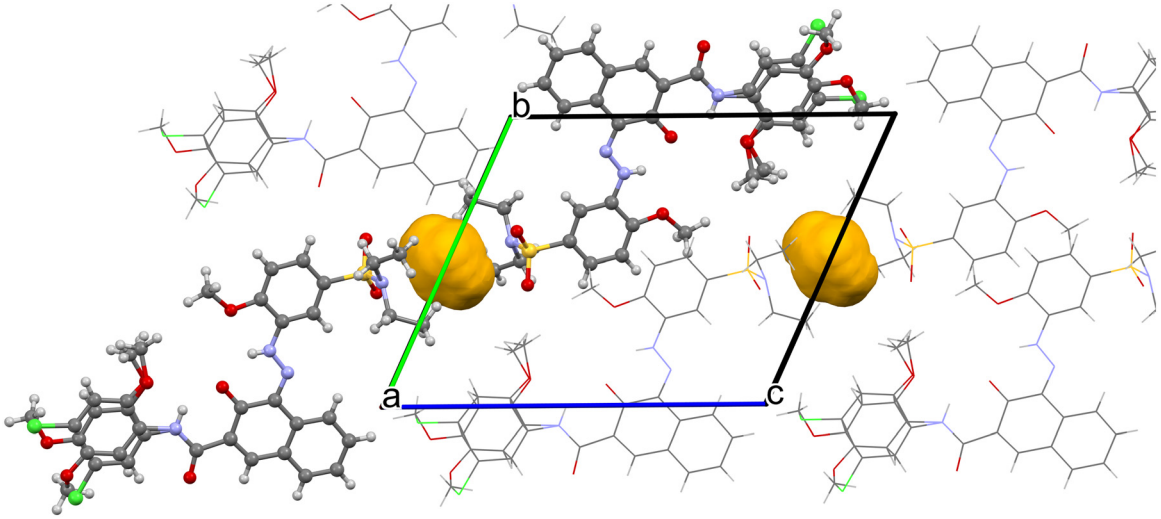

Fig. 19 Crystal structure of the mixed crystal of 71% of P.R.5 (**1**) and 29% if iso-P.R.5 (**3**). For a better comparison with Fig. 11 the unit cell was transformed to cell setting I.

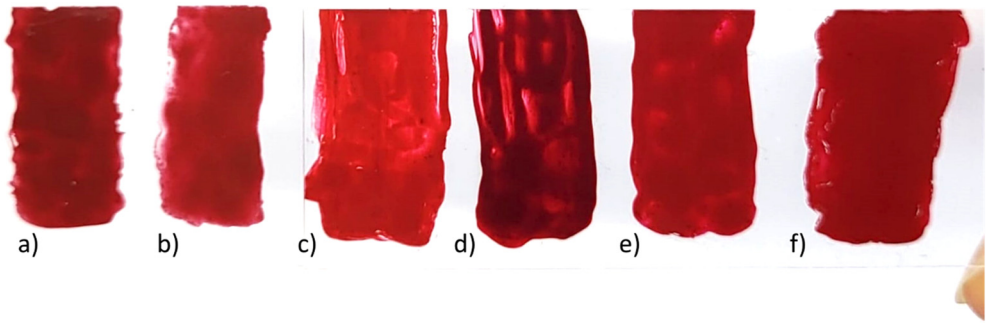

Fig. 20 Colour of Pigment Red 5 and several mixed crystals, shown as dispersions in linseed oil. (a) Mixed crystal of **1** + **2** + **3** + **4** (isostructural to the P.R.5 α-phase; obtained from a four compound 1 : 1 : 1 : 1 synthesis with subsequent heating in DMSO); (b) mixed crystal of **1** + **2** (isostructural to the α-phase of P.R.5, obtained from a 1 : 1 synthesis with subsequent heating in 1,2,4-trichlorobenzene); (c) commercial sample of the α-phase of Pigment Red 5 (**1**); (d) β-phase of Pigment Red 5; (e) mixed crystal of **1** + **2** + **3** + **4** (apparently isostructural to P.R.146, obtained by a four compound 1 : 1 : 1 : 1 synthesis with subsequent heating in xylene); and (f) commercial pigment red 146 (**4**).

obtained experimentally, disproving the calculation result. Apparently, it is worth trying the synthesis of a mixed crystal even if the lattice-energy calculations predict the impossibility of such attempts.

One of the main challenges during the crystallisation of the mixed crystals was the different solubility of the individual starting compounds, and the different solubilities of the individual pigments, which in some cases resulted in a fractionation of the compounds during synthesis and finish. For example, a cosynthesis of **1** + **2** + **3** + **4** with subsequent single-crystal growth did not lead to crystals of a quaternary solid solution, but of a solid solution of **1** + **3** only, as proven by SCXRD. In contrast, X-ray powder patterns proved that solid solutions of **1** + **2** + **3** + **4**, isostructural to P.R.5, can be obtained. In this solid solution, according to the lattice-energy minimisations, the void between the molecules should be filled.

It has long been known that the colours of organic pigments strongly depend on the crystal structure, and that different polymorphs may exhibit significantly different hues.[3] Also the two polymorphs of P.R.5 show different colours: the α-phase exhibits a bright red hue, whereas the β-phase has a dull shade, see Fig. 20c and d. The colours of three of the obtained solid solutions and of P.R.146 (**4**) are shown in Fig. 20, too. The desired bright red colour of α-P.R.5 could not be matched by its β-phase, by Pigment Red 146 or by the synthesized solid solutions, although the solid solutions shown in Fig. 20a and b are isostructural to P.R.5. Apparently, there is still room for optimisation.

5. Conclusion

Most inorganic and organic pigments are polymorphic. For P.R.5, no polymorphism was published hitherto. There was only one known polymorphic form (α-phase), which is also produced industrially. Starting from this phase, a polymorph screening was performed, which included heating suspensions in various solvents, dry heating, sublimation and melting experiments. No other polymorphic forms could be detected.

In contrast, historical records of the industrial producer Hoechst AG from 1979 indicate the existence of a second polymorph, which finally turned out to correspond to the crude product directly obtained from synthesis and was called "β-phase".

The α-phase is the thermodynamically stable phase, at least under the investigated conditions.

No additional polymorphs, solvates or hydrates were detected.

The crystal structure of the α-phase of P.R.5 was determined by 3-dimensional electron diffraction (3D-ED) on nanocrystalline material. Later, despite the pronounced insolubility of P.R.5 in all solvents even at elevated temperature, tiny needles could be grown, which were suitable for single-crystal X-ray diffraction (SCXRD). The ED-derived structure was fully corroborated by the SCXRD data, despite the different crystal morphologies and measurement temperatures. α-P.R.5 crystallises in the triclinic space group $P\bar{1}$ ($Z = 2$). The molecules exhibit the usual hydrazone tautomeric form with an essentially planar molecular geometry. The molecules are arranged in layers, which are stacked along the *a* axis.

Remarkably, the structure contains an intrinsic void of about 36 $Å^3$ between the SO_2NEt_2 groups of neighbouring stacks. Such a void is unprecedented among non-ionic commercial organic pigments and has never been observed in any phase of any non-ionic industrial organic pigment, despite more than 200 known crystal structures. Such a void implies reduced packing efficiency and a less stable lattice. Within the sensitivity of ED and SCXRD, there is no indication of water or solvent molecules occupying this site, so the void must be regarded as an intrinsic feature of the P.R.5 lattice. This observation is highly unexpected, because all commercial organic pigments are optimised on very dense molecular packings leading to good stabilities and application properties. A non-efficient packing leads to a deterioration of the properties. Indeed, the application properties of P.R.5 are sub-optimal.

To overcome these drawbacks of P.R.5, crystal engineering was applied to fill this void using suitably designed derivatives and mixed crystals (solid solutions). At first, possible derivatives and mixed crystals were investigated by lattice-energy minimisation. The modelling results identified several derivatives and mixed crystals isostructural to the α-phase of P.R.5. Subsequently, the most promising mixed crystals were synthesised and analysed by XRPD and SCXRD. Indeed, several mixed crystals were found which were isostructural to P.R.5, as evidenced by XRPD and, in selected cases, SCXRD. According to lattice-energy minimisations, in these solid solutions, the void was filled, as intended.

However, the differing solubilities of the components led in several systems to partial fractionation. For example, a four-component synthesis (molecules **1** + **2** + **3** + **4**) led to a single crystal, which, according to SCXRD, contained only two of the molecules (molecules **1** + **3**), which were unable to fill the void between them.

These results show the power of crystal engineering for the development of industrial organic pigments with tailored properties. The basis for the crystal engineering was laid by structure determination of P.R.5 by 3D ED and SCXRD.

This study demonstrates the power of 3D ED, in combination with laboratory SCXRD, XRPD and lattice-energy calculations, to resolve long-standing structural questions in commercially relevant organic pigments and to rationalise unusual packing features such as intrinsic voids. The structural insights into P.R.5, its polymorphism and its solid solutions provide a basis for correlating crystal packing with fastness properties and for the future design of pigment derivatives with improved application properties.

For future pigments developments, it is important to determine the crystal structure and to search for voids, which destabilize the lattice. This is especially valuable for cheap pigments with non-optimal properties (such as P.R.5), when there are indications that the properties might be considerably improved by a slight modification of the molecular structure, or by the formation of solid solutions. It is easier to search for the reason behind mediocre properties than to synthesize hundreds of derivatives blindly and test their properties with the hope of finding improved pigments, as it has been done in the past.

Crystal engineering has repeatedly been successfully applied to organic pigments. But crystal engineering requires the knowledge of the crystal structures and of the polymorphic forms. Regrettably, after more than 100 years of production and approximately 100 years of crystallographic research on organic pigments, there are still many commercial pigments, of which the polymorphism has never been investigated, and of which the crystal structure even of the commercial polymorph is not known. We hope that with the increasing power of ED and of other methods for structure determination of nanocrystalline compounds, the foundation for more crystal structure determinations and for the optimization of crystal engineering will be established.

Author contributions

Conceptualization: MUP; investigation: synthesis and crystallisation NL and SR, XRPD SR, polymorph screening and attempts to solve the crystal structure from powder data SR, electron diffraction TG, single-crystal X-ray analysis EH; formal analysis: crystal engineering idea MUP, modelling SR; resources: MUP, TG, EH; supervision: MUP; visualization: SR, TG; writing: MUP, SR, TG, EH.

Conflicts of interest

The authors declare no conflict of interest.

Data availability

All crystallographic information is contained in the supplementary information (SI) and the deposited cif files.

Supplementary information is available. See DOI: https://doi.org/10.1039/d6ce00140h.

CCDC 2498247, 2521903, 2527434, 2544539 and 2545237 contain the supplementary crystallographic data for this paper.[51a–e]

Acknowledgements

The authors thank Natalia Sennova (Goethe University, Frankfurt) for measuring the X-ray powder patterns. Toms Rekis (Goethe University, Frankfurt) is gratefully acknowledged for selecting and mounting the single crystal samples for X-ray analysis. SR thanks Barbara Scherer (Goethe University) for supporting the crystal modelling studies. Erich Paulus (formerly Hoechst AG, Frankfurt-Höchst, deceased) provided the historical powder patterns of P.R.5 polymorphs. We gratefully acknowledge Harald Schweitzer (formerly Hoechst AG, Frankfurt-Höchst) for the description of the powder diffractometer used in 1979. The authors thank the pigments department of Clariant (later Heubach, now Sudarshan, Frankfurt-Höchst) for providing samples of P.R.5, P.R.146, and the starting materials for the syntheses. EH gratefully acknowledges the DFG for financial support of this investigation (HA 5137/5 and HA 5137/7). We are grateful to Paul Klar (University of Bremen) for his support in dynamical refinement with JANA.

References

1 *Encyclopedia of color, dyes, pigments*, ed. G. Pfaff, Berlin Boston, De Gruyter, 2022.
2 Sudarshan, https://sudarshan.com, 2026.
3 K. Hunger, M. U. Schmidt, T. Heber, F. Reisinger and S. Wannemacher, *Industrial organic pigments: production, crystal structures, properties, applications*, Weinheim, Germany, Wiley-VCH, 2018.
4 A. Abel, The new colour index international of pigments and solvent dyes, *Surf. Coat. Int.*, 1998, **81**, 77–85.
5 A. Whitaker, The crystal structure of C.I. Pigment Red 2, 1′-(2,5-dichlorophenyl)azo-2′hydroxy-3′-phenylamidonaphthalene, *Z. Kristallogr., Kristallgeom., Kristallphys., Kristallchem.*, 1977, **146**, 173–184.
6 M. U. Schmidt, D. W. M. Hofmann, C. Buchsbaum and H. J. Metz, Crystal structures of Pigment Red 170 and derivatives, as determined by X-ray powder diffraction, *Angew. Chem., Int. Ed.*, 2006, **45**, 1313–1317.
7 J. L. Teteruk, J. Glinnemann, T. E. Gorelik, A. Linden and M. U. Schmidt, Explanation of the stacking disorder in the β-phase of Pigment Red 170, *Acta Crystallogr., Sect. B: Struct., Cryst. Eng. Mater.*, 2014, **70**, 296–305.
8 E. F. Paulus, Molecular and crystal structure of C.I. Pigment Red 208, 12514, *n*-butyl-2-{2-oxo-3-[*N*-(2-oxo-2,3-dihydro-5-benzimidazolyl)-carbamoyl]-naphthylidenhydrazino-benzoat (PV-Rot HF2B), *Z. Kristallogr.*, 1982, **160**, 235–244.
9 E. F. Paulus and K. Hunger, Über die Molekül- und Kristallstruktur eines roten Mono-"azo"-Pigmentes, *Farbe Lack*, 1980, **86**, 116–120.
10 C.-H. Chang, R. M. Christie and G. M. Rosair, C.I. Pigment Red 266, *Acta Crystallogr., Sect. C: Cryst. Struct. Commun.*, 2003, **59**, o556–o558.
11 C.-H. Chang, R. M. Christie and G. M. Rosair, The crystal structures of three azonaphtharylamide pigments, *Dyes Pigm.*, 2009, **82**, 147–155.
12 D. Kobelt, E. F. Paulus and W. Kunstmann, Röntgeneinkristallstrukturanalyse eines Chlorderivates von Permanentrot FRLL. Vergleich mit dem entsprechenden Derivat von Permanentbraun FG, *Z. Kristallogr., Kristallgeom., Kristallphys., Kristallchem.*, 1974, **139**, 15–32.
13 D. Kobelt, E. F. Paulus and W. Kunstmann, Röntgeneinkristallstrukturanalyse von 1-(2,5-dichlorphenylazo)-2-hydroxy-3-naphthoesäure-(4-chlor-2,5-dimethoxy-anilid) (Chlorderivat von Permanentbraun FG)®, *Acta Crystallogr., Sect. B*, 1972, **28**, 1319–1324.
14 J. Ribka, Monoazopigment, Verfahren zu seiner Herstellung und Verwendung, German Patent DE 2043482C, 1970.
15 S. N. Kabekkodu, A. Dosen and T. N. Blanton, PDF-5+: a comprehensive Powder Diffraction File™ for materials characterization, *Powder Diffr.*, 2024, **39**, 47–59.
16 I. J. Bruno, J. C. Cole, P. R. Edgington, M. Kessler, C. F. Macrae, P. McCabe, J. Pearson and R. Taylor, New software for searching the Cambridge Structural Database and visualizing crystal structures, *Acta Crystallogr., Sect. B: Struct. Sci.*, 2002, **58**, 389–397.
17 M. Gemmi, E. Mugnaioli, T. E. Gorelik, U. Kolb, L. Palatinus, P. Boullay, S. Hovmöller and J. P. Abrahams, 3D electron diffraction: the nanocrystallography revolution, *ACS Cent. Sci.*, 2019, **5**, 1315–1329.
18 L. Palatinus, P. Brázda, M. Jelínek, J. Hrdá, G. Steciuk and M. Klementová, Specifics of the data processing of precession electron diffraction tomography data and their implementation in the program *PETS2.0*, *Acta Crystallogr., Sect. B: Struct. Sci., Cryst. Eng. Mater.*, 2019, **75**, 512–522.
19 W. Kabsch, XDS, *Acta Crystallogr., Sect. D: Biol. Crystallogr.*, 2010, **66**, 125–132.
20 G. Winter, D. G. Waterman, J. M. Parkhurst, A. S. Brewster, R. J. Gildea, M. Gerstel, L. Fuentes-Montero, M. Vollmar, T. Michels-Clark, I. D. Young, N. K. Sauter and G. Evans, *DIALS*: implementation and evaluation of a new integration package, *Acta Crystallogr., Sect. D: Struct. Biol.*, 2018, **74**, 85–97.
21 C. J. Gilmore, J. A. Kaduk and H. Schenk, *International Tables for Crystallography. H: Powder Diffraction*, Chichester, Wiley, 2019.
22 T. Gorelik, M. U. Schmidt, J. Brüning, S. Bekő and U. Kolb, Using electron diffraction to solve the crystal structure of a laked azo pigment, *Cryst. Growth Des.*, 2009, **9**, 3898–3903.
23 M. U. Schmidt, S. Brühne, A. K. Wolf, A. Rech, J. Brüning, E. Alig, L. Fink, C. Buchsbaum, J. Glinnemann, J. Van De Streek, F. Gozzo, M. Brunelli, F. Stowasser, T. Gorelik, E. Mugnaioli and U. Kolb, Electron diffraction, X-ray powder diffraction and pair-distribution-function analyses to determine the crystal structures of Pigment Yellow 213, $C_{23}H_{21}N_5O_9$, *Acta Crystallogr., Sect. B: Struct. Sci.*, 2009, **65**, 189–199.

24 T. E. Gorelik, S. Habermehl, A. A. Shubin, T. Gruene, K. Yoshida, P. Oleynikov, U. Kaiser and M. U. Schmidt, Crystal structure of copper perchlorophthalocyanine analysed by 3D electron diffraction, *Acta Crystallogr., Sect. B: Struct. Sci., Cryst. Eng. Mater.*, 2021, **77**, 662–675.

25 T. E. Gorelik, C. Czech, S. M. Hammer and M. U. Schmidt, Crystal structure of disordered nanocrystalline α^{II}-quinacridone determined by electron diffraction, *CrystEngComm*, 2016, **18**, 529–535.

26 T. E. Gorelik, S. L. Bekő, J. Teteruk, W. Heyse and M. U. Schmidt, Analysis of diffuse scattering in electron diffraction data for the crystal structure determination of Pigment Orange 13, $C_{32}H_{24}Cl_2N_8O_2$, *Acta Crystallogr., Sect. B: Struct. Sci., Cryst. Eng. Mater.*, 2023, **79**, 122–137.

27 Y. Krysiak, S. Plana-Ruiz, L. Fink, E. Alig, U. Bahnmüller, U. Kolb and M. U. Schmidt, High temperature electron diffraction on organic crystals: *In situ* crystal structure determination of Pigment Orange 34, *J. Am. Chem. Soc.*, 2024, **146**, 9880–9887.

28 Farbenfabriken Bayer Aktiengesellschaft, Wasserunlösliche Azofarbstoffe und Verfahren zu deren Herstellung, German patent disclosure No. 1444665.2, 1968.

29 A. Boultif and D. Louër, Indexing of powder diffraction patterns for low-symmetry lattices by the successive dichotomy method, *J. Appl. Crystallogr.*, 1991, **24**, 987–993.

30 W. I. F. David, K. Shankland, J. Van de Streek, E. Pidcock, W. D. S. Motherwell and J. C. Cole, *DASH*: a program for crystal structure determination from powder diffraction data, *J. Appl. Crystallogr.*, 2006, **39**, 910–915.

31 I. Nederlof, E. Van Genderen, Y.-W. Li and J. P. Abrahams, A Medipix quantum area detector allows rotation electron diffraction data collection from submicrometre three-dimensional protein crystals, *Acta Crystallogr., Sect. D: Biol. Crystallogr.*, 2013, **69**, 1223–1230.

32 B. L. Nannenga, D. Shi, A. G. W. Leslie and T. Gonen, High-resolution structure determination by continuous-rotation data collection in MicroED, *Nat. Methods*, 2014, **11**, 927–930.

33 T. Gorelik, MRC to TIFF converter, 2023, DOI: 10.5281/ZENODO.7936068.

34 G. M. Sheldrick, A short history of *SHELX*, *Acta Crystallogr., Sect. A: Found. Crystallogr.*, 2008, **64**, 112–122.

35 G. M. Sheldrick, Crystal structure refinement with *SHELXL*, *Acta Crystallogr., Sect. C: Struct. Chem.*, 2015, **71**, 3–8.

36 O. V. Dolomanov, L. J. Bourhis, R. J. Gildea, J. A. K. Howard and H. Puschmann, *OLEX2*: a complete structure solution, refinement and analysis program, *J. Appl. Crystallogr.*, 2009, **42**, 339–341.

37 V. Petříček, L. Palatinus, J. Plášil and M. Dušek, Jana2020– a new version of the crystallographic computing system Jana, *Z. Kristallogr. - Cryst. Mater.*, 2023, **238**, 271–282.

38 G. M. Sheldrick, *SHELXT*– Integrated space-group and crystal-structure determination, *Acta Crystallogr., Sect. A: Found. Adv.*, 2015, **71**, 3–8.

39 C. B. Hübschle, G. M. Sheldrick and B. Dittrich, *ShelXle*: a Qt graphical user interface for ISHELXL, *J. Appl. Crystallogr.*, 2011, **44**, 1281–1284.

40 *Materials Studio*, Accelrys Software Inc, 2008.

41 S. L. Mayo, B. D. Olafson and W. A. Goddard, DREIDING: a generic force field for molecular simulations, *J. Phys. Chem.*, 1990, **94**, 8897–8909.

42 J. Gasteiger and M. Marsili, Iterative partial equalization of orbital electronegativity—a rapid access to atomic charges, *Tetrahedron*, 1980, **36**, 3219–3228.

43 S. M. Hammer, R. Panisch, M. Kobus, J. Glinnemann and M. U. Schmidt, Simulation of absorption sites of acetone at ice: (0001) surface, bulk ice and small-angle grain boundaries, *CrystEngComm*, 2009, **11**, 1291.

44 B. Scherer, R. Himmler and M. U. Piepenbring, *Inclusion of byproducts and additives in the crystal lattice of quinacridone*, soon to be published.

45 N. S. Osborne, H. F. Stimson and D. C. Ginnings, Measurements of heat capacity and heat of vaporization of water in the range 0 degrees to 100 degrees C, *J. Res. Natl. Bur. Stand.*, 1939, **23**, 197.

46 C. J. E. Kempster and H. Lipson, A rapid method for assessing the number of molecules in the unit cell of an organic crystal, *Acta Crystallogr., Sect. B*, 1972, **28**, 3674–3674.

47 D. W. M. Hofmann, Fast estimation of crystal densities, *Acta Crystallogr., Sect. B: Struct. Sci.*, 2002, **58**, 489–493.

48 L. Glasser, The effective volumes of waters of crystallization: general organic solids, *Acta Crystallogr., Sect. B: Struct. Sci., Cryst. Eng. Mater.*, 2020, **76**, 650–653.

49 M. U. Schmidt, M. Ermrich and R. E. Dinnebier, Determination of the structure of the violet pigment $C_{22}H_{12}Cl_2N_6O_4$ from a non-indexed X-ray powder diagram, *Acta Crystallogr., Sect. B: Struct. Sci.*, 2005, **61**, 37–45.

50 E. F. Paulus, F. J. J. Leusen and M. U. Schmidt, Crystal structures of quinacridones, *CrystEngComm*, 2007, **9**, 131–143.

51 (*a*) CCDC 2498247: Experimental Crystal Structure Determination, 2026, DOI: DOI: 10.5517/ccdc.csd.cc2pvmmt; (*b*) CCDC 2521903: Experimental Crystal Structure Determination, 2026, DOI: DOI: 10.5517/ccdc.csd.cc2qn7qc; (*c*) CCDC 2527434: Experimental Crystal Structure Determination, 2026, DOI: DOI: 10.5517/ccdc.csd.cc2qv04r; (*d*) CCDC 2544539: Experimental Crystal Structure Determination, 2026, DOI: DOI: 10.5517/ccdc.csd.cc2rdsxw; (*e*) CCDC 2545237: Experimental Crystal Structure Determination, 2026, DOI: DOI: 10.5517/ccdc.csd.cc2rfjf5.